Characterizing the Role of Phospholamban in Duchenne Muscular Dystrophy

by

Emma Sara Juracic

A thesis

presented to the University of Waterloo

in fulfillment of the

thesis requirement for the degree of

Master of Science

in

Kinesiology

Waterloo, Ontario, Canada, 2018

AUTHOR'S DECLARATION

I hereby declare that I am the sole author of this thesis. This is a true copy of the thesis, including any required final reversions, as accepted by my examiners.

I understand that my thesis may be made electronically available to the public.

ABSTRACT

Duchenne muscular dystrophy (DMD) and the murine model, *mdx*, are recessive X-linked myopathies characterized by aberrant Ca^{2+}-handling resulting in muscle atrophy and weakness. Phospholamban (PLN) is a protein inhibitor of sarco(endo)plasmic reticulum Ca^{2+}-ATPases (SERCAs) that physically interacts with SERCA to regulate Ca^{2+}-handling. Targeted therapy to improve SERCA function is a proven strategy to alleviate DMD in *mdx* mice. In this study, *Pln*$^{-/-}$ mice were crossed with *mdx* mice to generate *mdx*/*Pln*$^{-/-}$ double knockout mutant mice. Since PLN inhibits SERCAs, it was hypothesized that PLN ablation would mitigate Ca^{2+} dysregulation and rescue the dystrophic phenotype. Soleus and diaphragm muscles from WT, *mdx/Pln*$^{+/+}$ and *mdx/Pln*$^{-/-}$ mice were excised to determine differences in the muscle morphology and functionality. Histological analysis revealed stark increases in the proportion of centralized nuclei and collagen invasion in *mdx/Pln*$^{-/-}$ and *mdx* mice compared to WT, however, there were no differences in these markers between *mdx* groups. Immunofluorescence staining demonstrated that both soleus and diaphragm from *mdx/Pln*$^{-/-}$ mice shifted towards type IIB and type IIX fibre types, as the proportion of these fibres were significantly greater than *mdx/Pln*$^{+/+}$ and WT. This shift was accompanied by increased cross sectional area of type IIB fibres in *mdx/Pln*$^{-/-}$ compared to *mdx/Pln*$^{+/+}$. Western blotting analysis of soleus and diaphragm muscle homogenate showed an increase inexpression of the SERCA regulator, sarcolipin (SLN), in both *mdx* groups relative to WT, however, there was a significant decline in SLN content in *mdx/Pln*$^{-/-}$ compared to *mdx/Pln*$^{+/+}$. Additionally, there was a significant elevation in PLN content in *mdx/Pln*$^{+/+}$ relative to WT in the soleus muscle. The solei of *mdx/Pln*$^{+/+}$ and *mdx/Pln*$^{-/-}$ mice exhibited a significant reduction in force production compared to their WT counterparts at all frequencies when normalized to cross sectional

area. Unexpectedly, the force generated by *mdx/Pln*$^{-/-}$ soleus was significantly decreased at all stimulation frequencies when compared to *mdx/Pln*$^{+/+}$. Furthermore, there was a significant reduction in soleus and diaphragm Ca^{2+} uptake in both the *mdx/Pln*$^{+/+}$ and *mdx/Pln*$^{-/-}$ groups compared to WT, and surprisingly the rate of Ca^{2+} uptake was significantly lower in *mdx/Pln*$^{-/-}$ muscles compared with *mdx/Pln*$^{+/+}$. Interestingly, while there were differences in SERCA mediated Ca^{2+} uptake between experimental groups, there were no significant differences in Ca^{2+}- ATPase activity between WT, *mdx/Pln*$^{+/+}$ and *mdx/Pln*$^{-/-}$ groups in the soleus and diaphragm muscles. Overall, these results demonstrate that PLN ablation in the *mdx* mouse model resulted in a worsening of the disease phenotype, as evident by elevations in centralized nucleation, a reduction in the ability to generate force and impairments in SERCA mediated Ca^{2+} uptake. These results suggest that PLN could potentially provide stabilization of the SERCA structure and function during oxidative stress.

ACKNOWLEDGEMENTS

First and foremost, I would like to thank my supervisor, Dr. Russ Tupling, for taking the chance on a random student that contacted him much too late to even be considered. Russ, I don't know what you saw in me that persuaded you to offer me a place in your lab but I am very grateful you did. Being a part of this lab has been the highlight of my academic career and I can't begin to express how happy I am that I will have the next four (or five, according to Eric) years to continue to learn from you and grow as both a researcher and a person.

I would like to also thank my committee members: Dr. Joe Quadrilatero and Dr. Robin Duncan, for their assistance and guidance over the last two years, both in a lab and classroom setting. I look forward to continuing to learn from your mentorship as I transition into my PhD.

Eric, "lab dad", thank you for fixing the things that I break; for putting up with my never-ending questions and "terrible" music; for always waiting for me so that we can get our morning coffee together (even if that means waiting forever in that Tim Hortons line). Your support and encouragement has been instrumental to the completion of this thesis. Thank you for always pushing me to do better and for reminding me that I am "no better than an undergrad" when I think too highly of myself. But most importantly, thank you for supporting my pizza habit.

Dan, thank you for being an outstanding mentor and friend. For taking the time to not only teach me techniques but for having faith in me when I was unsure of myself. I can't thank you enough for the guidance and support you've given me and continued to give me even though you're on the other side of the country. I hope to inspire future students the way you have inspired me.

To my lab mates: Dr. Val Fajardo, Paige Chambers, Catherine Bellissimo, Gabbi Lugod (aka the RTAngels), Riley Sonnenburg, and Brad Rietze – you all have made the past two years so wonderful and special. The Tupling lab definitely has a welcoming sense of family and it has made every day so very enjoyable. I've looked forward to coming into the lab each day and I owe that to all of you! As we go our separate ways, I look forward to the great things you will accomplish but know that we all will always be Tupling4Life! I must also thank everyone on the physiology floor, it has been a pleasure to work alongside each of you.

To my family and friends, thank you for being proud of me even though you had no idea what I've been doing for the past two years. I am extremely fortunate to call a very special group of people my friends. You all mean so much to me. Thank you to my parents and brothers for their unwavering and unconditional patience, support and encouragement. To my best friend, Grace, you honestly deserve an honorary MSc for keeping me organized and on track. I cannot thank you enough for listening to me constantly talk science for the past two years, for listening to me complain, for encouraging me when I doubted myself and for celebrating my accomplishments (as small as they were sometimes).

DEDICATION

This thesis is dedicated to my parents Marina and Perica, and brothers Emanuel and Borna. I owe my love of science to my mother: when young girls were receiving Barbie's, I was receiving anatomy coloring books. Mama, I am so glad you encouraged me to pursue a future in science. The last two years have been tumultuous at times, but knowing that I could turn to each of you for support has meant the world to me. Whether I needed a laugh or a cry, a word of encouragement or a stern talking to, you were all always there for me and for that I am truly thankful. I couldn't have done this without you.

Table of Contents

List of Tables

List of Figures

List of Abbreviations

Ca^{2+} - Calcium
$[Ca]_i$ - Intracellular Ca^{2+} concentration
$[Ca]_f$ - Free Ca^{2+} concentration
CCCP - Carbonyl cyanide m-chlorophenyl hydrazone
DIA - Diaphragm
DGC - Dystroglycan complex
DHPR - Dihydropyridine receptors
DMD - Duchenne muscular dystrophy
ECC - Excitation-contraction coupling
EDL - Extensor digitors longus
HSP70 - Heat shock protein 70
mdx - murine model of Duchenne muscular dystrophy
MLN - Myoregulin
NFAT - Nuclear factor of activated T-cells
PLN - Phospholamban
PP1 - Protein phosphatase 1
ROS - Reactive oxygen species
RyR - Ryanodine receptor
SACs - Stretch activated channels
SERCA - Sarco(endo)plasmic reticulum Ca^{2+}-ATPase
SLN - Sarcolipin
SOL - Soleus
SR - Sarco(endo)plasmic reticulum
SUMO - Small ubiquitin-related modifier
TRPC - Transient receptor potential channel
utr - Utrophin
V_{max} - Maximum velocity

Introduction

Phospholamban (PLN) is a critical regulator of muscular Ca^{2+} homeostasis, as it modulates the activity of the sarco(endo)plasmic reticulum Ca^{2+}-ATPase (SERCA), a crucial Ca^{2+}-handling protein situated on the sarcoplasmic reticulum (SR). The interaction between these two proteins and the biological function of PLN have been characterized comprehensively in mammalian cardiac muscle. In studies examining cardiac tissue, ablation of PLN or adrenergic stimulation of PLN phosphorylation (see details below), acts to increase SERCA activity and enhance myocyte relaxation rates and contractility [1, 2]. Conversely, overexpression of PLN in cardiac muscle can cause superinhibition of SERCA, and induce congenital heart failure due to a lethal depression in SR Ca^{2+}- handling [3-6]. Investigations into the role of PLN in a dystrophic environment have been primarily limited to cardiomyopathies. These investigations have highlighted the crucial role of Ca^{2+} dysregulation in myocyte contractile dysfunction and dystrophic disease progression [7]. Furthermore, these studies have yielded promising results in the murine model, as PLN ablation improved Ca^{2+}- handling and consequently alleviated symptoms of the myopathy while impeding disease progression [8, 9]. However, the role of PLN in healthy and diseased mammalian skeletal muscle is much less clear. It has been shown conclusively that PLN is expressed in the mouse soleus, where it regulates SERCA activity [10]. Based on the knowledge that PLN is a critical Ca^{2+}-handling protein in healthy and diseased cardiac tissue, PLN and its interaction with SERCA in skeletal muscle warrants further investigation to gain a fuller understanding of Ca^{2+} homeostasis in skeletal muscle health and disease.

Ca^{2+} Homeostasis in Skeletal Muscle

Calcium (Ca^{2+}) is regarded as a universal intracellular messenger that is essential for nearly all aspects of cell life [11-13]. Conceptually, its action is relatively simple: at basal levels, the intracellular Ca^{2+} concentration ($[Ca^{2+}]_i$) is maintained below 100 nM, however, a rise in this concentration to 1000 nM (or greater) triggers cellular activation through the induction of numerous second messenger pathways [11, 12]. The maintenance of a low resting $[Ca^{2+}]$ is critical to normal cell function, and as such, Ca^{2+} levels are tightly controlled [13]. In skeletal muscle specifically, this regulation is achieved primarily by the SR, as well as, by key contributions from sarcolemmal proteins, cytoplasmic buffers and mitochondria [14-16]. The SR is an intracellular tubular network, that while analogous to the endoplasmic reticulum, functions as the dynamic Ca^{2+} regulator in muscle and serves to provide automatic feedback control for altering and maintaining both cytosolic and luminal $[Ca^{2+}]$ [14-16]. It accomplishes this through the collective effort of three major classes of Ca^{2+} - regulating proteins: luminal calcium binding proteins (calsequestrin), Ca^{2+} - release channels (ryanodine receptor; RyR), and the SERCA Ca^{2+} - reuptake pumps [14-16].

With the SR being so intrinsically tied to Ca^{2+} homeostasis, it comes as no surprise that it is pivotal in the induction of both muscle contraction, otherwise known as excitation-contraction coupling (ECC), and muscle relaxation [17]. The sequence of events that initiate skeletal muscle contraction begin with an action potential propagating along the plasma membrane, and depolarizing the transverse-tubule system, where the electrical stimulus is detected by the dihydropyridine receptors (DHPRs) and converted to a chemical one through an allosteric interaction with RyR, that triggers the release of Ca^{2+} [18]. The transient elevation in $[Ca^{2+}]_i$ binds to troponin C, causing a conformational change that removes the inhibitory action of

tropomyosin and enables the formation of cross bridges between actin and myosin in order to generate force [18]. Subsequently, muscle relaxation is elicited by the active transport of Ca^{2+} from the cytosol to the SR lumen by SERCA, in order to restore the luminal SR Ca^{2+} stores for ensuing contractions and to return cytosolic $[Ca^{2+}]_i$ to basal levels [18]. SERCA activity is not limited to SR re-filling. The SERCA pumps are additionally vital in maintaining resting $[Ca^{2+}]_i$ under basal conditions by counteracting passive Ca^{2+} leak either through RyR or the pumps themselves, thus keeping a tight control of Ca^{2+} levels.

The molecular diversity of these Ca^{2+} - regulatory proteins govern basal $[Ca^{2+}]_i$, as well as, contraction and relaxation properties of different muscle fibre types [19, 20]. Slow twitch muscle fibres (fibres expressing slow or type I myosin) exhibit higher resting $[Ca^{2+}]_i$ compared to fast twitch fibres (fibres expressing fast or type II myosin) [21-23]. Additionally, this is accompanied by complete saturation of the luminal SR Ca^{2+} store, whereas, fast twitch fibre SR content is only 35% of its capacity at basal levels [21]. This is directly related to the variable density of protein expression between fibre types. Fast twitch muscle fibres express 3-5-fold greater DHPR and RyR content, thus facilitating an accelerated Ca^{2+} release [19, 21, 24]. Moreover, these fibres exhibit a 5-7-fold greater density of SERCA, which ensures faster and more efficient Ca^{2+} clearance [21, 25]. Lastly, fast twitch fibres express increased calsequestrin content that enables a greater luminal SR Ca^{2+} capacity [21, 25, 26]. Consequentially, the Ca^{2+} transient in fast twitch muscle fibres is greater and shorter compared to slow twitch fibres and this results in faster contraction kinetics and greater force production [21]. These characteristics not only highlight the differences in muscle fibre composition, but the diverse effects that could be imposed by the dysregulation of Ca^{2+} - handling proteins. While it is the concerted action of multiple Ca^{2+} - regulating proteins that maintains skeletal muscle Ca^{2+} homeostasis, this thesis

will focus on the interaction between SERCA and one of its regulatory proteins, PLN, in both healthy and diseased states.

SERCA Structure and Function

SERCAs are 110-kDa integral membrane transporter proteins embedded within the SR that consist of a single polypeptide chain which arranges into the transmembrane and cytosolic regions [27]. The transmembrane region is composed of 10 α-helices (M1-M10) of differing lengths and properties, in which SERCA's two Ca^{2+} binding sites reside within helices M2, M4, M6 and M9 [27, 28]. Crystal structure analysis has demonstrated that these two Ca^{2+} binding sites are located adjacent to each other and near the cytoplasmic surface of the lipid layer. In fact, the Ca^{2+} binding sites are only accessible from the cytoplasmic side of the SR, thus prohibiting the binding of luminal Ca^{2+} [15, 29]. The transmembrane region is connected to the large cytosolic headpiece, consisting of three domains: the ATP or nucleotide binding domain; the phosphorylation domain which is phosphorylated by the γ-phosphate of ATP at a conserved aspartate residue; and the actuator domain which is integral to the de-phosphorylation event, as assisted by a conserved glutamate [27, 28]. Phosphorylation of the SERCA protein, due to binding of ATP, induces a conformational change of the transmembrane helices that transfers bound Ca^{2+} from the cytoplasm to the SR lumen [15]. SERCA belongs to the P-type ATPase (P-ATPase) superfamily of ion transporters due to its α-helical structure, its ability to catalyze ATP and its ability to undergo a reversible conformational shift between two states, denoted E_1 and E_2 [15, 30]. The SERCA family itself is encoded by the *ATP2A1-3* genes which are located on 3 different chromosomes and code for the expression of SERCA1, SERCA2 and SERCA3 isoforms respectively, with further isoform diversity occurring through alternative splicing [30]. These isoforms are highly conserved, retaining 75% structural homology despite differences in

species-specific and muscle-specific expression [30]. The SERCA isoform variants of particular interest in muscle health and disease are SERCA1a and SERCA2a. SERCA1a is the primary isoform in adult fast-twitch skeletal muscle and has been demonstrated to have a vital role in skeletal muscle development [30]. In contrast, SERCA2a is predominantly expressed in cardiac muscle and slow-twitch skeletal muscle [30]. Additional SERCA isoform variants include SERCA2b, which is expressed at low levels in all tissues, and SERCA3, which is expressed in numerous non-muscle tissues [15].

SERCAs use the free energy released from the hydrolysis of ATP to transport Ca^{2+} ions from the cytosol into the lumen of the SR; and as such, are major regulators of $[Ca^{2+}]_i$ [31]. SERCA – mediated Ca^{2+} transport necessitates multiple steps and conformational changes to the pump [15]. Transport begins with the SERCA pump in its E_1 conformational state and the binding of Ca^{2+} to its high-affinity sites on the cytoplasmic face of the transmembrane domain [32]. Occupation of these sites induces ATP hydrolysis and this triggers SERCA phosphorylation and a change in conformation to the E_2 state [32]. This state exhibits reduced Ca^{2+} affinity and thus Ca^{2+} dissociates from the pump and enters the SR lumen [32]. Under optimal conditions, the pump can transport two molecules of Ca^{2+} at the expense of one ATP molecule [15, 31]. However, this ratio is subject to change depending on a number of factors including: $[Ca^{2+}]_i$, ATP level, pH, ADP and inorganic phosphate level. These factors can have an influence on SERCA Ca^{2+} affinity, ATP binding and subsequent hydrolysis, phosphorylation of the pump, and the return of the pump to the E_1 conformation. Additionally, SERCA activity is modulated by numerous protein regulators, including myoregulin (MLN) and DWORF, however, the two best understood are the functionally homologous SR integral membrane proteins: PLN and sarcolipin (SLN) [33].

Phospholamban

PLN is a 52-amino acid monomeric protein composed of a long hydrophilic, NH_2-terminal, cytoplasmic domain and a short hydrophobic, transmembrane, COOH-terminal domain [33-35]. Its quaternary structure is organized into three domains: cytosolic domain Ia (amino acids 1-20) that houses the phosphorylation sites Ser^{16} and Thr^{17}; cytosolic domain Ib (amino acids 21-30); and transmembrane domain II (amino acids 31-52) [36]. In its unphosphorylated state, PLN physically interacts with SERCA to reduce its apparent Ca^{2+} affinity, while exhibiting little to no effect on the V_{max} measured at saturating [Ca^{2+}] [35, 37]. The inhibitory effect of PLN on SERCA function can be observed as a rightward shift in the Ca^{2+} curve of enzyme activation and has been documented in SR vesicles prepared from all mammalian species examined to date, including murine, canine and human samples [33-35, 37]. PLN monomers have been observed to oligomerize into noninhibitory homopentamers, however, the function of these homopentamers is not yet understood [35, 37]. Conditions of high $[Ca^{2+}]_i$ or adrenergic stimulation will induce phosphorylation of PLN, as cAMP-dependent protein kinase A will target Ser^{16} and Ca^{2+}/calmodulin-dependent kinase II will target Thr^{17} to relieve the inhibition [35, 37, 38].

The interaction between SERCA and PLN has been shown to occur at three sites:

i) a cytoplasmic interaction site produced by charged and hydrophobic amino acids in PLN cytosolic domain Ia and by amino acids Lys-Asp-Asp-Lys-Pro-Val402 in SERCA2a [39-41]

ii) a cytoplasmic interaction site, formed by the PLN cytosolic domain Ib [39-41]

iii) the SERCA transmembrane domain; and the PLN transmembrane domain II/SERCA transmembrane helix M6 interaction site [39-41]

These interaction sites are highly conserved between SERCA1 and SERCA2 isoforms, and as such, SERCA1 and SERCA2 co-expression with PLN in COS-1 cells has demonstrated an identical reduction in Ca^{2+} affinity in the presence of PLN [35].

Studies examining how PLN exerts its inhibitory effect on SERCA have been conflicting. It has been suggested that the binding of PLN to SERCA renders the pump catalytically inactive and that PLN dissociation is required for activation [37, 39, 42-44]. Conversely, other studies suggest that PLN is a subunit of SERCA and as such remains bound to the pump throughout the catalytic cycle [37, 45-47]. Recently, Akin & Jones (2012) have confirmed that PLN exclusively binds to the E_2 SERCA conformation (specifically, residues Gln^{23} to Leu^{52} interact with the groove formed between transmembrane helices M2, M4, M6 and M9 of the pump) and that PLN competes with Ca^{2+} for binding to the pump by stabilizing SERCA in the E_2 state and thus inhibiting the formation of the E_1 conformation [37, 42]. Due to this, at low $[Ca^{2+}]$, SERCA is essentially catalytically inactive, however, increases in the $[Ca^{2+}]$ completely inhibit the interaction between PLN and SERCA (as the binding of Ca^{2+} to SERCA closes the groove with which PLN interacts) and induces a conformational change to the E_1 state [37, 42]. This seems to suggest that PLN dissociation from the pump is required for catalytic activation and subsequent Ca^{2+} transport. Indeed, this is corroborated by increases in Ca^{2+}-ATPase activity and Ca^{2+} uptake in the absence of PLN interaction with SERCA [37]. However, this does not explain the effects of PLN phosphorylation on this interaction. MacLennan and his team have been instrumental in advancing our understanding of this and have demonstrated that while the physical interaction between PLN and SERCA is dissociated by elevations in $[Ca^{2+}]$, PLN phosphorylation relieves the inhibitory interaction without physical dissociation of the two proteins [39-42]. According to their model, the transmembrane domain remains tethered to SERCA, while the cytoplasmic

domain exists in an equilibrium between three different conformational states: a stable inhibitory T state, an intermediate excited R state, and an uninhibitory B state [39-42]. PLN phosphorylation shifts the equilibrium towards the B state, thus relieving inhibition, while maintaining physical interaction between the pump and its regulatory protein [39-42]. NMR spectroscopy in combination with mutant PLN studies have corroborated this model and have illustrated that the phosphorylation of PLN disrupts only the functional interaction while leaving the physical interaction intact [39-42].

In human cardiac muscle, PLN is predominately expressed in the ventricle where it regulates the activity of SERCA2a, whereas, in human skeletal muscle, PLN has been shown to regulate both SERCA1a and SERCA2a, with a preference for SERCA2a [10, 48]. In murine muscle, PLN content is significantly reduced when compared to human levels, however, the expression pattern is similar, as PLN has been found in both the left ventricle and slow twitch muscles, such as the soleus [1]. The regulatory role of PLN in cardiac tissue has been extensively investigated. In the heart, the physiological role of SERCA2a is to modulate the rate of clearance of cytosolic Ca^{2+} and the capacity of the luminal SR Ca^{2+} load, and as such, is crucial in cardiac relaxation and contraction [36, 49, 50]. PLN acts as the intersection point between two signal transduction pathways: the β - adrenergic signalling pathway (that allows for protein phosphorylation) and the Ca^{2+} - signalling pathway (that initiates contraction), through which it can modulate SERCA2a activity, therefore regulating cardiac relaxation and contraction [36]. In murine models, the absence of PLN in cardiac tissue resulted in a linear increase in SERCA affinity for Ca^{2+}, as well as, linear increases in contractile properties (such as myocyte cell shortening, contraction rate and re-lengthening) and improved relaxation rates [36]. In fact, PLN ablation mimicked the maximal stimulation contraction and relaxation rates of wild-type hearts

[36]. Conversely, overexpression of PLN in murine cardiac tissue resulted in reduced rates of contraction and relaxation, as well as, decreases in the amplitude of the Ca^{2+} signal and an extended decay of the Ca^{2+} transient [36].

It comes as no surprise that the relationship between PLN and SERCA is a key component of mammalian heart failure [36, 51-53]. Under this pathophysiological condition, the expression of SERCA2a is reduced while PLN content remains unaffected, thus altering the PLN:SERCA2a ratio. In addition, the phosphorylation of PLN declines [36]. Consequently, PLN's inhibitory role is enhanced, thus mimicking the results observed with PLN overexpression, with impairments in Ca^{2+} uptake and contractile dysregulation [36]. Interestingly, ablation of PLN in murine heart failure models improves myocardial inotropy and lusitropy, hence rescuing the phenotype and alleviating the disorder [36]. However, the same cannot be said for human heart failure, as PLN is a crucial factor in human cardiac health and its absence induces lethal heart failure [36, 51]. PLN mutant studies have revealed that reductions in expression or loss of function mutations in the PLN gene lead to either severe or delayed cardiomyopathy in humans, depending on the extent of the mutation [51]. For example, in hereditary instances of cardiomyopathy, a T116G point mutation has been identified in the PLN cDNA that causes a substitution of a termination codon for Leu-39 (L39stop) [51]. Consequentially, cardiac tissue of inflicted individuals can show over a 50% reduction in PLN mRNA, as well as, low-to-no detectable PLN protein [51]. Individuals that are homozygous for this mutation develop severe dilated cardiomyopathy and heart failure that can only be rescued by cardiac transplantation [51]. Heterozygous individuals exhibit delayed cardiomyopathy, characterized by hypertrophy and prolonged impairments in contractile properties [51]. A possible explanation for the discrepancy between murine and human models of heart failure

could be attributed to differences in cardiac use and in the mechanisms regulating cardiac function [51, 54-57]. The mouse heart beats approximately 10 times faster than the human heart, beating approximately 600 times per minute. Therefore, the mechanisms regulating the contractile and relaxation properties differ between species [51, 54-57]. In the mouse heart, the clearance of Ca^{2+} is solely dependent upon SERCA2a, whereas, in the human heart, SERCA2a accounts for only two thirds of this clearance, as the Na^{+}/Ca^{2+} exchanger removes the remainder. Additionally, there are differences in the ventricular motor proteins [51, 54-57]. In adult mouse heart tissue, α-myosin heavy chain predominates, whereas, in adult human cardiac tissue the β-myosin heavy chain predominates [51, 54-57]. It has been suggested that due to the demand placed on mouse cardiac muscle (and the subsequent mechanistic changes incurred) that the mouse heart is operating near its theoretical maximum and as such PLN deletion is not as deleterious when compared to the slower beating human heart [51].

While there have been efforts to understand the role of PLN in cardiac muscle, a characterization of PLN in both healthy skeletal muscle and in skeletal muscle disease progression has been lacking. Our lab has explicitly demonstrated that PLN is expressed in mouse soleus muscle, where it exerts an inhibitory effect on both SERCA1a and SERCA2a [10]. Therefore, it is reasonable to expect that PLN's physiological role in cardiac tissue can be inferred in skeletal muscle as well. Furthermore, this implies that PLN could be a potential target in skeletal muscle diseases that stem from abnormal Ca^{2+} - handling, such as Duchenne Muscular Dystrophy (DMD) (see below), as PLN may play a vital component of skeletal muscle Ca^{2+} homeostasis as is seen in cardiac muscle.

Duchenne Muscular Dystrophy and Dystrophin

Muscular dystrophies are a heterogeneous population of inherited disorders which present a variety of clinical, genetic and biochemical features [58]. These disorders are characterized by elevated levels of muscle turnover which manifest in the progressive atrophy of axial, limb and facial muscles [58, 59]. Within this population, DMD presents as the most common and severe form and thus has garnered the most attention. DMD is inherited as a recessive X-linked disorder, affecting predominately males and resulting in fatal weakening and wasting of skeletal, respiratory and cardiac muscles [58]. It is caused by a lack of the dystrophin protein, primarily due to out-of-frame deletions within the large dystrophin gene, or less commonly due to nonsense mutations [59]. Affected individuals appear healthy at birth with the onset of clinical signs (muscle weakness and impaired mobility) occurring between the ages of two to four. The aggressive nature of this myopathy leaves individuals wheelchair bound before adolescence and the development of respiratory and cardiac complications arise shortly thereafter. Despite extensive investigation into the genetic and cellular characteristics of this disorder, an effective treatment remains elusive, such that those affected do not survive past the age of twenty [58, 60, 61].

Dystrophin itself is a 110 nm long, rod-shaped cytoskeletal protein that is predominately expressed in muscle. It is located at the inner surface of muscle fibres where it serves as a vital component of the dystroglycan complex (DGC), which functions to form a critical link between the submembrane cytoskeleton and components of the extracellular matrix. This link requires dystrophin to bind to γ -actin and β -dystroglycan, which in turn, binds to laminin via α -dystroglycan [62]. This critical link confers structural stability to the sarcolemmal membrane, as well as offers the sarcolemma protection during times of muscle contraction and relaxation.

Moreover, as depicted in Table 1 below, the DGC, and specifically dystrophin, have significant roles in the regulation of numerous signaling pathways in skeletal muscle. This highlights the breadth of signalling pathways and signalling molecules confirmed to associate with the DGC, including: nNOS, ion and water channels, protein and lipid kinases, transporters and G protein receptors [62]. However, perhaps most important, is the fact that the DGC, in association with caveolin, regulates signaling pathways that initiate nitric oxide production, Ca^{2+} influx and reactive oxygen species (ROS) production. These pathways are of particular relevance to the pathophysiology of DMD, as they underlie the onset and progression of this myopathy [62].

Table 1: Signaling Proteins Associated with the Dystroglycan Complex in Skeletal Muscle

Protein	Function	DGC Binding Site
nNOS/NOS1	Ca^{2+}/calmodulin-dependent NO synthesis	α-Syntrophin, Dystrophin
ARMS	EphA4 receptor-associated protein and a substrate for ephrin receptors	α-Syntrophin
Mixed-lineage leukemia 5, MLL5	Regulator of myogenin expression	α-Syntrophin
PTEN	Phosphatase and tensin homolog; dephosphorylates PIP_3 to PIP_2	α-Syntrophin
Nav 1.4, Nav 1.5	Skeletal and cardiac muscle sodium channels	α-Syntrophin
Kir2.1, Kir4.1	Inward rectifier potassium channels	Syntrophins (multiple)
TRPC1, TRPC4	Non-voltage-gated cation channels	α-Syntrophin
Diacylglycerol kinase zeta	Metabolizes diacylglycerol to phosphatidic acid	γ1- and α-Syntrophin
Stress-activated kinase 3, ERK6, p38γ	Mitogen-activated protein kinase	α-Syntrophin
MAST205	Microtubule-associated serine/threonine kinase	β2-Syntrophin
Src kinase	Non-receptor tyrosine kinase	β-Dystroglycan
Myocilin	Modulator of muscle hypertrophy pathway	α-Syntrophin

Adapted from: Allen, D.G., Whitehead, N.P. & Froehner, S.C. (2016) Absence of Dystrophin Disrupts Skeletal Muscle Signaling: Roles of Ca^{2+}, Reactive Oxygen Species and Nitric Oxide in the Development of Muscular Dystrophy. *Physiological Reviews,* 96: 253–305

mdx Murine Model of DMD

In order to understand disease progression and the corresponding mechanisms, the most accepted animal model of DMD is the *mdx* mouse [63, 64]. This mouse line arose from a

spontaneous mutation in an inbred line of C57BL/10 mice and these mice possess a nonsense mutation in exon 23 of the dystrophin gene which abolishes dystrophin expression in all tissues [63-65]. *mdx* mice show minimal indications of the myopathy until approximately three – four weeks of age, at which point they undergo extensive myofibre degeneration that targets essentially all fibres [63, 66]. Subsequently, *mdx* muscle sustains continuous cycles of muscle turnover (muscle degeneration and regeneration) that is accompanied by elevations in inflammation and fibrosis [63, 67, 68]. In general, at the age of ten weeks, muscle turnover and inflammation subside in the limb muscles but remain high in the diaphragm [63, 68]. The incurred muscle turnover can be histopathologically represented by the appearance of regenerated myofibers which exhibit centrally localized nuclei, as well as, by a rise in heterogeneity in myofiber cross-sectional area [63].

As a compensatory mechanism, affected *mdx* muscles have been observed to undergo a fast-to-slow fibre type shift; a transition that is necessitated because this myopathy preferentially targets fast twitch fibres (type IIB and IIX) [69-71]. Type IIB fibres have been shown to be the first to suffer degeneration, and in fact, the majority of these fibres experience numerous cycles of muscle fibre turnover prior to the onset of slow twitch fibre necrosis [69]. This pattern is not specific to DMD, but has additionally been observed in disorders including central core disease, nemaline myopathy and congenital fibre type disproportion [69]. Increasing the proportion of slow twitch fibres is considered adaptive because these fibres exhibit a three to four-fold increase in expression of the dystrophin-related protein, utrophin, compared to fast twitch fibres [71, 72]. Utrophin is a cytoskeletal protein that shares a high degree of resemblance to dystrophin, including the actin and glycoprotein binding domains as well as hinge regions and spectrin-like repeats. In mature skeletal muscle fibers, utrophin is preferentially expressed at the

neuromuscular junction, however, utrophin is not only limited to junctional regions and its expression levels can be altered depending on the state of the muscle fibre: myogenic differentiation, muscle denervation and muscle degeneration have been shown to modulate utrophin expression [70-72]. Over-expression of utrophin has been demonstrated to ameliorate the dystrophic phenotype in both murine and canine models of the disease [71, 73-76]. Moreover, over-expressing the upstream regulators of utrophin, such as PGC-1α, has proven to rescue the dystrophic phenotype by inducing the transition from type IIB and IIX fibres to type I and IIA fibres [71].

The published literature on the structural and functional properties of *mdx* muscle has illustrated that the dystrophic environment hinders muscle contractile properties [77-79]. In examining the extensor digitors longus (EDL) and SOL muscles of *mdx* and healthy counterparts, Lynch *et al*. (2001) have demonstrated that these *mdx* muscles are pseudo-hypertrophic, in that the isometric force of the twitch and the tetanus are elevated relative to healthy muscle, but, upon normalization to muscle mass or cross sectional area, force is significantly reduced [78, 79]. This is further exacerbated in EDL, due to the higher proportion of type IIB fibres and their increased susceptibility to damage, as both damaged and regenerating fibres have been shown to develop less force per unit of cross-sectional area and less force per unit mass [78, 79]. The pseudo-hypertrophy of dystrophic muscle has been associated with an increase in non-contractile tissue, such as connective and fibrotic tissue, which acts to preserve muscle structure at the expense of functional properties, including force production [78, 79].

In comparison to the human form of DMD, the *mdx* model appears relatively benign, as these mice evade the end – stage lethal histopathologic symptoms and the functional disability observed in the human pathology [63, 67]. Additionally, these mice share the lifespan of normal

C57BL/10 mice and appear to behave normally [63, 67]. Other murine models of DMD have been studied, including the *mdx:utr* $^{-/-}$ and *mdx:utr* $^{-/+}$ models. The *mdx:utr* $^{-/-}$ mice lack utrophin, in addition to dystrophin, and as such represent a much more severe form of the myopathy that more closely resembles the severity of the human version, however, these mice show a very limited lifespan of approximately two – three months, and thus are inappropriate models for examining longevity and prolonged disease progression [63, 73]. The *mdx:utr* $^{-/+}$ model has recently garnered much attention, as these mice exhibit a prolonged lifespan while maintaining an intermediate dystrophic pathology [63, 80, 81]. Utrophin expression in these mice is reduced, which facilitates a more severe pathology as compared to the *mdx* model. Despite the shortcomings of the *mdx* model, it remains the most widely used and has facilitated much insight into the underlying mechanisms and progression of the myopathy.

Duchenne Muscular Dystrophy and Ca^{2+} Dysregulation

It is not yet fully understood how the absence of dystrophin renders muscle susceptible to damage and degradation, however, two main theories have been proposed:

1. Dystrophin acts to maintain the integrity of the sarcolemmal membrane during contractions, especially contractions that induce stretch, and without dystrophin, these contractions can result in membrane tears [60, 61, 82].
2. Dystrophin may have an important protein scaffolding role and aid in the localization and regulation of membrane ion channels. The absence of dystrophin may impair channel formation and/or function [60, 61, 82].

These theories are not mutually exclusive and both suggest that the absence of dystrophin would cause an elevation in intracellular Ca^{2+} concentration ($[Ca^{2+}]_i$), leading to a dysregulation of Ca^{2+} homeostasis and the induction of numerous degradative pathways that lead to successive cycles

of muscle fibre degeneration and regeneration, chronic inflammation, fibrosis and eventual muscle cell necrosis [60, 62]. In the absence of dystrophin, the formation of the DGC is impaired, such that the critical link between the cytoskeleton and the extracellular matrix is lost. Furthermore, an additional consequence of the loss of dystrophin is the 80-90% reduction in expression of dystrophin-associated proteins, all of which are constituents of the DGC [60-62, 83]. As a result, the architecture of the sarcolemmal membrane is functionally altered and this could allow for the development of "transient membrane tears" during muscle contraction [60, 82]. The induction of these tears is corroborated by the appearance of localized cell damage in association with localized membrane damage; leakage of soluble proteins, such as creatine kinase, from the cell into the plasma; and increases in $[Ca^{2+}]_i$ as a result of Ca^{2+} influx through damaged membranes [61]. However, as Allen *et al*. (2010) noted, the above support for the presence of membrane tears can also be accounted for by increased stretch induced membrane permeability [61]. In order to distinguish between membrane tears and other causes of membrane permeability, researchers have artificially induced "holes" in the membrane and examined the properties and repairs of defects. Bansal *et al*. (2003) have illustrated that in both healthy tissue and in murine models which exhibit a mild DMD phenotype (*mdx*), repair of such defects occurred in less than one minute [84]. What was not considered in this previous study was the frequency by which these membrane tears occur in *mdx* tissue compared with healthy tissue. Evidence shows that *mdx* tissue is at least six times more likely to exhibit transient membrane tears than healthy tissue [85]. Thus while repair may occur in a similar timely fashion after single injury, membrane damage is considerably more persistent in dystrophic muscle and this could affect the ability of the cell to repair continual damage and could alter the aggregation of membrane ion channels [85].

The incurred membrane instability has been reported to contribute to the increased sarcolemmal permeability to extracellular Ca^{2+}. A secondary feature to the induction of membrane tears is the presence of transient and highly localized influxes of Ca^{2+}, deemed Ca^{2+} entry "hot spots" [60, 85]. The persistent influx of Ca^{2+} through these hot spots promotes membrane insertion of Ca^{2+} leak channels through an exocytotic pathway, as well as, activates the Ca^{2+} dependent proteases needed to stimulate these channels, thus resulting in a self-perpetuating damage pathway [60, 85]. In addition to the greater open probability of Ca^{2+} leak channels in dystrophic tissue, stretch activated channels (SACs) have been implicated in the aberrant Ca^{2+} signaling observed in this myopathy. Muscle fibres of young *mdx* mice have shown increases in activity and density of these channels in the sarcolemma which precede the initial markers of muscle damage and necrosis, potentially indicating a role of these channels in the onset of the pathology [60]. While the identity of the channel(s) has not been determined, experimental findings have proposed the canonical transient receptor potential channel (TRPC) to be a potential candidate. TRPC1, TRPC4 and TRPC6 have been identified as components of the sarcolemma in vertebrate skeletal muscle and the inhibition of TRPC1 and TRPC4 in *mdx* muscle reduced Ca^{2+} influx [60, 61, 86, 87]. Dysregulation of these channels stems from the absence of dystrophin. As mentioned previously, dystrophin binds to β-dystroglycan, which among other proteins, can bind to caveolin-3, the scaffolding protein of the caveolae [61, 62, 86]. While most of the proteins comprising the DGC are reduced in expression in DMD, caveolin-3 shows increased expression and the caveolae themselves are increased in frequency but disordered in location [86, 88]. Caveolae are critical in the aggregation of key proteins to allow for interaction and regulation of membrane protein channels including: L-type Ca^{2+} channels, Na^{+} channels, K^{+} channels, the Na/Ca exchanger, SRC kinase, PLC, nNOS, and TRPC1 [86, 89,

90]. It is thought that the absence of dystrophin results in improper structure and function of the caveolae which consequently alters the formation and behavior of the membrane channels with which it interacts [86].

Studies conducted on muscles from the *mdx* mouse, have demonstrated the extent of $[Ca^{2+}]_i$ overload and its corresponding influence on the progression of necrosis and muscle degeneration [61, 91-94]. Most significantly, work conducted by Goonasekara *et al.* (2011) has demonstrated that increased Ca^{2+} influx into the sarcoplasm alone is sufficient to induce a DMD-like phenotype [95]. The implication of $[Ca^{2+}]_i$ overload is primarily the induction of numerous detrimental process which further exacerbate the disease. Elevated $[Ca^{2+}]_i$ has been demonstrated to activate both proteolytic calpains and caspases, increase ROS production, promote mitochondrial apoptosis, increase inflammation and stimulate fibrosis [96-100]. Dystrophic skeletal muscle exhibits increases in caspase and calpain activity during times of both muscle degeneration and regeneration [60]. As a result, these muscles show elevated rates of protein degradation, upwards of 80% greater, compared to healthy counterparts, leading to progressive atrophy and muscle weakness. Reducing the abnormal $[Ca^{2+}]_i$ in *mdx* tissue to levels resembling that of healthy tissue, reverts the rate of proteolysis back to normal levels and improves the myopathy [60, 97, 101].

Additionally, mitochondria isolated from dystrophic tissue exhibit greater swelling as a response to sustained elevations in $[Ca^{2+}]_i$. Consequently, these mitochondria are more prone to rupturing and causing necrotic and/or apoptotic cell death. Genetically altering mitochondria to be insensitive to Ca^{2+} overload, and thus preventing Ca^{2+}-induced swelling, in a dystrophic environment has been shown to provide protection from cell death and a reduction in myofibre necrosis [98]. Mitochondrial Ca^{2+} overload has also been implicated in impairments in oxidative

phosphorylation which contributes to greater ROS production [60]. This elevation in production, coupled with increased vulnerability of *mdx* tissue to ROS damage, results in greater lipid peroxidation and oxidation of proteins [60, 102]. ROS-mediated lipid peroxidation has been shown to increase membrane permeability and to precede the onset of necrosis in dystrophic tissue, thus suggesting that ROS may have a primary role in the induction of muscle degeneration [60, 102]. ROS have been additionally implicated in the activation of NF-κB, a transcription factor that is essential in the regulation of inflammation and immunity [60, 96]. NF-κB gene targets, including the pro-inflammatory cytokines TNF-α , IL-1β, IL-6, and iNOS have been reported to be up-regulated in dystrophic tissue [96, 103]. TNF-α further perpetuates ROS damage as it can act on the mitochondria to stimulate ROS production, thus creating a detrimental positive feedback loop, in which increased ROS induces further cell damage and activation of NF-κB [60, 96]. In addition to membrane instability, there is evidence that these Ca^{2+} damage pathways can also be attributed to impediments in the removal of Ca^{2+} from the sarcoplasm, possibly due to reduced expression or abnormal function of the SERCA pumps [104-106].

SERCA and Ca^{2+} Dysregulation in Duchenne Muscular Dystrophy

SERCAs are redox-sensitive proteins that exhibit a high vulnerability to oxidative damage and inactivation, so much so, that the modification of a single cysteine residue is sufficient for the alteration of activity [15, 107-109]. It has been well documented that SERCAs undergo considerable oxidative stress in the dystrophic environment and as such are functionally altered through post-translational modifications, particularly nitrosylation [110] . These modifications reduce maximal SERCA activity due to modifications in the Ca^{2+}-binding and ATP-binding domains which consequently change SERCA enzyme kinetics. As such, the

regulatory role of SERCA has been demonstrated to be impaired in the DMD myopathy [105, 106, 111]. Kargacin & Kargacin (1996) have established the extent of this SERCA dysregulation, in which Ca^{2+} sensitivity of SERCA is maintained while the maximum velocity of SR Ca^{2+} uptake is reduced [106]. This finding has been corroborated in murine models which exhibit a mild DMD phenotype (*mdx*) as well as a more severe, lethal phenotype (*mdx:utr -/-*) [112]. Research conducted by Schneider *et al.* (2013) has elaborated on the differences in expression of SERCA isoforms and their corresponding functional alterations in both the *mdx* and *mdx:utr -/-* models. This group has determined that there is muscle specific variability in protein levels: SERCA1a expression is significantly reduced in the diaphragm but remains unaltered in the soleus and quadriceps; whereas, SERCA2a expression is significantly increased in the quadriceps but is unaltered in the soleus and diaphragm muscles [112]. However, despite the variation in protein levels, both SERCA isoforms exhibited significant reductions in Ca^{2+} uptake [112]. This highlights the degree of SERCA dysregulation in a dystrophic environment, both in terms of expression and functional impairments and the abnormal Ca^{2+}- handling that is incurred as a consequence.

A popular method of ameliorating the aberrant Ca^{2+}signaling observed in DMD is through SERCA overexpression, which has been applied to different SERCA isoforms, as well as to different muscles, including the soleus and diaphragm [95, 104]. SERCA overexpression acts to mitigate Ca^{2+} dysregulation and, consequently, has been shown to diminish the dystrophic phenotype [95, 104]. In multiple studies, the overexpression of SERCA1 served to reduce Ca^{2+} influx and inhibit $[Ca^{2+}]_i$ overload. As a result of this, there were significant reductions in disease markers, including centrally localized nuclei, muscle fibrosis, serum creatine kinase levels, mitochondrial swelling and calpain activation [95, 104]. A different approach aimed at

stabilizing SERCA function has also proven to be an effective therapeutic strategy for normalizing levels of $[Ca]_i$ and improving the DMD phenotype. Through the use of Hsp70, a molecular chaperone protein which possesses the ability to physically interact with SERCA and preserve its function Gehrig *et al*. (2012) have demonstrated that preventing SERCA damage acts to improve Ca^{2+}-handling and mitigate the dystrophic phenotype [107, 110]. This speaks to the importance of targeting Ca^{2+} dysregulation to alleviate symptoms of the myopathy and impede disease progression, and shows that SERCA has a central role in this approach.

Sarcolipin

SERCA activity is modulated by numerous protein regulators, however, the two best understood are the functionally homologous SR integral membrane proteins: PLN (as previously discussed) and sarcolipin (SLN) [33]. PLN and SLN share common patterns of expression, as both proteins are expressed in the heart, with PLN regulating SERCA2a in the ventricle and SLN regulating SERCA2a in the atria [48]. Furthermore, both proteins are present in skeletal muscle and are both capable of regulating both SERCA1 and SERCA2 activity [33,10]. SLN is composed of 31 amino acids and expresses transmembrane, cytoplasmic and luminal domains [112,48]. SLN physically binds to SERCA and acts to reduce the apparent affinity of SERCA for Ca^{2+} and to inhibit SERCA Ca^{2+} uptake [33,10,38]. Additionally, SLN possesses the ability to uncouple ATP hydrolysis from SERCA Ca^{2+} transport, which enables it to mediate skeletal muscle adaptive thermogenesis [28]. Recently, the emerging role of SLN in Ca^{2+} homeostasis and disease progression in the dystrophic environment has been comprehensively examined. Schneider *et al.* have reported increases in SLN expression in dystrophic muscle which may contribute to the development of SERCA dysfunction [112]. Whereas, Voit *et al.* (2017) have corroborated the increase in SLN protein density in the myopathy and furthermore, have

demonstrated that the elevation in protein expression is detrimental to SERCA function and further propagates the disease phenotype [113]. It was shown that the reduction or ablation of SLN expression in the *mdx:utr* $^{-/-}$ model served to improve SERCA function, as evident by a restoration of Ca^{2+} uptake and V_{max} to rates similar to the wild type control [113]. Subsequently, the improvement in Ca^{2+} handling in the dystrophic environment resulted in decreases in necrosis and fibrosis, prevention of the maladaptive fibre type transition to type IIB fibres, and improvements in force generation and grip strength [113]. Overall, these results clearly demonstrate that restoring SERCA function in this myopathy is critical to alleviating the aberrant Ca^{2+} homeostasis and mitigating the disease. With the structural and functional homology shared by PLN and SLN, it would be appropriate to investigate the role of PLN in the dystrophic environment in order to gain a fuller understanding of the importance of SERCA and its associated regulatory proteins in skeletal muscle disease.

Research Purpose

The objective of this study was to characterize the role of PLN in DMD. Specifically, this study aimed to assess the differences in the morphology and functionality of SOL and DIA muscles in *mdx/Pln*$^{-/-}$, *mdx/Pln*$^{+/+}$ and *Pln*$^{+/+}$ (WT) mice to establish the role of PLN in the myopathy and evaluate whether the absence of PLN will improve SERCA activity and mitigate the aberrant Ca^{2+} handling associated with this pathology.

Objectives

i) To investigate if the ablation of PLN will improve SERCA function in the *mdx/Pln*$^{+/+}$ phenotype to that of WT mice as evidenced by improvements in Ca^{2+} uptake and a leftward shift in the ATPase assay

ii) To examine if the absence of PLN will reduce the proportion of centralized nuclei and amount of fibrosis in *mdx/Pln*$^{+/+}$ muscle to levels resembling to that of WT mice, as this would be indicative of improved muscle morphology

iii) To determine if the generation of force produced by the SOL muscle is improved in *mdx/Pln*$^{+/+}$ mice lacking PLN and if it is comparable to the force production of WT mice, which would be suggestive of improved muscle function

Hypotheses

i) In the absence of PLN, SERCA function will be enhanced in *mdx/Pln*$^{-/-}$ mice compared to *mdx/Pln*$^{+/+}$ mice, and will resemble that of WT mice, such that there will be faster rates of Ca^{2+} uptake (at both maximum and physiologically relevant Ca^{2+} concentrations) and ATPase activity will be improved.

ii) The *mdx/Pln*$^{-/-}$ mice will have improved muscle morphology compared to the *mdx/Pln*$^{+/+}$ mice. This will be evident through the reductions in disease markers, including centralized nuclei and fibrosis, to levels that are comparable to WT and are indicative of decreased levels of muscle degeneration and regeneration.

iii) Muscle function in the *mdx/Pln*$^{-/-}$ mice will be improved compared to the *mdx/Pln*$^{+/+}$ mice. This will be exhibited by increases in twitch and tetanic force and faster rates of force development and relaxation. These contractile properties will be similar to the force production and rates of contraction and relaxation of WT mice.

Methods

Animals

Refer to Appendix A for greater detail regarding the breeding strategy. In short, the *Pln*$^{-/-}$ mice used to establish the *mdx/Pln*$^{-/-}$ colony were generated from heterozygous breeding pairs (*Pln*$^{+/-}$) previously purchased from Mutant Mouse Regional Resource Centers. Homozygous *Pln*$^{-/-}$ males from this colony were crossed with homozygous *mdx* females ($X^{mdx}X^{mdx}$) purchased from the Jackson Laboratory. The resultant F1 progeny consisted of heterozygous *mdx* females ($X^{mdx}X$) and hemizygous *mdx* males ($X^{mdx}Y$), all of which were heterozygous for *Pln* (*Pln*$^{+/-}$). Subsequently, from the F1 progeny, the hemizygous *mdx* females were crossed with heterozygous *mdx* males to yield the experimental *mdx* and *mdx/Pln*$^{-/-}$ mice. The experimental groups consisted of: *mdx/Pln*$^{-/-}$, *mdx/Pln*$^{+/+}$ and WT mice. From these groups, this study only examined homozygous male mice aged 4 to 6 months and biochemical analyses were restricted to the soleus, diaphragm and left ventricle tissues. The experimental animals were housed in an environmentally controlled room, under a reverse light/dark cycle (12/12 hr) in group cages and had access to food and water *ad libitum*. All experiments were reviewed and approved by the University of Waterloo Animal Care Committee in accordance with the Canadian Council on Animal Care.

Histology/Immunofluorescence

Mice aged 4 – 6 months were euthanized and immediately following, intact, whole diaphragm and soleus muscles were removed, mounted in O.C.T compound (Tissue-Tek) and then frozen in liquid nitrogen-cooled isopentane. Serial cross sections of tissue (10 μm thick) were then cut with the use of a cryostat (Thermo Electronic) maintained at -20°C and mounted onto slides. These slides were utilized to conduct either Hemotoxylin and Eosin (H&E) staining,

Van Geison staining or immunofluorescence. H&E staining was performed to visualize centrally localized nuclei. The Van Geison stain was used to determine the degree of fibrosis. A brightfield Nikon microscope linked to a PixeLink digital camera was used to acquire the images produced by the stains, and these images were quantified with ImageJ software. Immunofluorescence analysis was employed to assess muscle fibre type, satellite cell mobilization and inflammatory response. It was conducted according to the protocol established by Bloemberg *et al*. (2012) using primary antibodies from Developmental Studies Hybridoma Bank against the differing myosin heavy chain (MHC) isoforms: MHCI (BA-F8), MHCIIa (SC-71) , MHCIIb (BF-F3), whereas, MHCIIx fibres were unstained and appeared black. [114]. The secondary antibodies for immunofluorescence staining were Alexa Fluor 350 anti-mouse IgG2b, Alexa Fluor 488 anti-mouse IgG1, and Alexa Fluor 555 anti-mouse IgM, which were obtained from Molecular Probes. The images were acquired with the use of the Axio Observer Z1 fluorescent microscope equipped with red, green and blue filters, the AxioCam HRm camera and AxioVision Software (Carl Ziess). ImageJ software was used to quantify the images.

Western Blotting

The protein expression levels of PLN and SLN were assessed using standard western blotting techniques. Upon excision, the muscle samples were detendonized and weighed to determine muscle mass. These samples were then homogenized 1:10 (w/v) in ice-cold homogenizing buffer (250 mM sucrose, 5 mM HEPES, 0.2 mM PMSF and 0.2% [w/v] NaN_3) using a glass homogenizer and stored at -80°C. Subsequently, these muscle homogenates were solubilized into a 1x solubilizing buffer (0.1% 2-Mercaptoethanol, 0.0005% Bromophenol blue, 10% Glycerol, 2% SDS, and 63 mM Tris-HCl (pH 6.8)) and the proteins were electrophoretically separated with the use of a tricine based SDS-PAGE (13% total acrylamide

for PLN and SLN). Upon electrophoresis, the separated proteins were transferred onto polyvinylidene difluoride (PVDF) membrane (PLN) or nitrocellulose membrane (SLN) with transfer buffer (25 mM glycine, 192 mM Tris base, 20% methanol, 0.1% [w/v] SDS). The membranes were then incubated in blocking solution (TBST buffer: 20mM Tris base, 137 mM NaCl, and 0.1% (v/v) Tween 20, pH 7.5, with 5% [w/v] non-fat dry milk) to prevent non-specific binding. It is at this point that the proteins were immunoprobed with the corresponding primary antibodies for PLN ((MA3-922) monoclonal mouse antibody acquired from Pierce Antibodies) and SLN (polyclonal rabbit antibody acquired from Lampire Biological Laboratories). Subsequently, the proteins were immunoprobed with horseradish peroxidase-conjugated secondary antibodies: goat anti-mouse IgG (PLN) and goat anti-rabbit IgG (SLN), which were obtained from Santa Cruz Biotechnology. Luminata Forte™ was used to detect PLN and SuperSignal West Femto™ substrate (Pierce, Thermo Fisher Scientific Inc) was used to detect SLN. GeneTools (Syngene) was utilized to quantify the resulting optical densities. All values were normalized to protein content as determined from ponceau staining.

Muscle Contractility Analysis

Electrical stimulation and muscle contractility analysis was conducted on adult (6 month) *mdx/Pln*$^{-/-}$, *mdx* and *Pln*$^{+/+}$ mice. Intact, whole soleus muscles were excised and mounted in a bath composed of oxygenated Tyrode solution (95% O_2, 5% CO_2) containing 121 mM $NaCl_2$, 5 mM KCl, 24 mM $NaHCO_3$, 1.8 mM $CaCl_2$, 0.4 mM NaH_2PO_4, 5.5 mM glucose, 0.1 mM EDTA, and 0.5 mM $MgCl_2$, pH 7, and maintained at 25°C. The muscles were positioned between two platinum electrodes driven by a biphasic stimulator (Model 710B, Aurora Scientific, Inc.) and electrically stimulated muscle force was measured across a variety of stimulation frequencies, ranging from 1 to 100 Hz. The collected data were analyzed using Dynamic Muscle Control Data

Acquisition software (Aurora Scientific, Inc). The specific parameters that were assessed are peak isometric force amplitude (mN) and maximal rates of force generation (+d*F*/d*t*) and relaxation (-d*F*/d*t*). Upon completion, muscle length was measured and the muscle was removed from the bath, detendonized, and weighed to normalize the measurements to muscle mass.

SERCA Function Analysis

Assessment of SERCA function was conducted on soleus and diaphragm homogenates and was measured using Ca^{2+}-ATPase assays as previously described [115]. Briefly, Ca^{2+} -dependent SERCA activity was measured at Ca^{2+} concentrations ranging from pCa 7.0 to 3.5 using a plate reader assay on a spectrophotometer. GraphPad Prism was used to generate activity curves by non-linear regression curve fitting using a general sigmoidal model for substrate activity. SERCA activity was measured in the presence of Ca^{2+} ionophore A23187 (Sigma C7522) to mitigate any back inhibition as a result of SR vesicle filling [115]. Ca^{2+} uptake was determined in the presence of a precipitating anion, oxalate, with the use of the fluorescent dye Indo-1 in a spectrofluorometer that employs a monochromator to maintain the excitation wavelength at 355nm and two photomultiplier tubes to detect light emitted at 405 and 485nm. Rates of Ca^{2+} uptake were assessed at free [Ca^{2+}] ranging from the physiologically relevant [Ca^{2+}] of 100 nM to a [Ca^{2+}] of 1000 nM.

Statistics

The data are presented as means ± standard error. Unless otherwise stated, all statistical analyses were conducted using a one-way ANOVA to compare between groups (*mdx/Pln*$^{-/-}$, *mdx/Pln*$^{+/+}$, WT). Statistical significance is set at $p < 0.05$. Trending statistical significance is defined as $0.05 < p < 0.1$. Graph Pad Prism Statistical Software was used for all final image generation. Statistica4 Software was used for all statistical analysis.

Results

Animal Physical Characteristics

Adult WT, *mdx/Pln*$^{+/+}$, and *mdx/Pln*$^{-/-}$ mice were sacrificed at 4-6 months and weighed thereafter. The body weight of *mdx/Pln*$^{-/-}$ mice was significantly lower compared to *mdx/Pln*$^{+/+}$ ($p = 0.01$) and WT ($p = 0.05$). SOL muscles were excised and de-tendonized prior to weighing. SOL weight was significantly higher in both *mdx/Pln*$^{+/+}$ ($p = 0.01$) and *mdx/Pln*$^{-/-}$ ($p = 0.009$) relative to WT. SOL weight was not different between *mdx* groups.

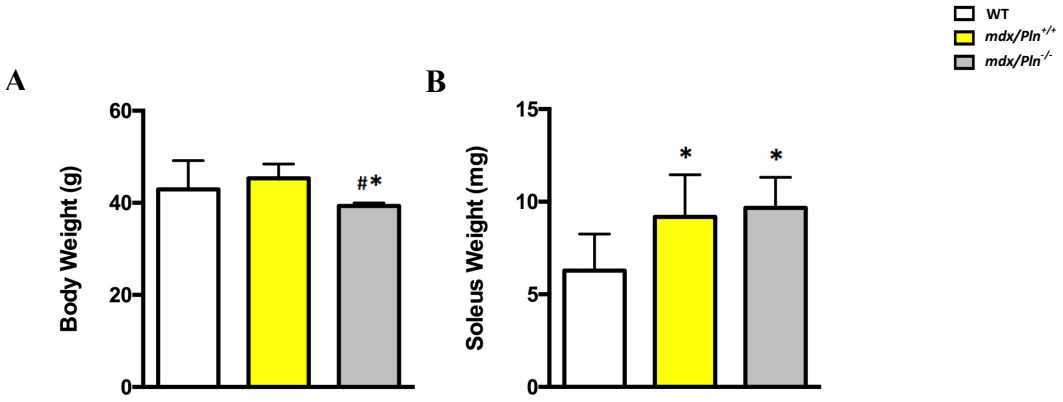

Figure 1. Body weight and soleus weight in WT, *mdx/Pln*$^{+/+}$ and *mdx/Pln*$^{-/-}$ mice. (A) Body weight and **(B)** soleus weight in WT (n = 12), *mdx/Pln*$^{+/+}$ (n = 12) and *mdx/Pln*$^{-/-}$ (n = 12) mice. * indicates a significant difference from WT ($p < 0.05$) and # indicates a significant difference from *mdx/Pln*$^{+/+}$ ($p < 0.01$).

Histological and Immunofluorescent Properties

Centralized nuclei data from H&E staining are shown in Fig. 2. In SOL, the proportion of centralized nuclei in the *mdx/Pln*$^{+/+}$ and *mdx/Pln*$^{-/-}$ mice was significantly greater ($p < 0.0002$) compared to their WT counterparts (Fig. 2B). There was also a trend ($p < 0.09$) for higher centralized nuclei count in *mdx/Pln*$^{-/-}$ compared to *mdx/Pln*$^{+/+}$ (Fig. 2B). Similarly, in DIA, the *mdx/Pln*$^{+/+}$ and *mdx/Pln*$^{-/-}$ mice exhibit significantly greater ($p < 0.0002$) centralized nuclei than WT, however, there were no differences between the *mdx* groups (Fig. 2C).

Fibrosis data from Van Gieson staining are shown in Fig. 3. Fibrosis in the SOL was significantly elevated ($p < 0.05$) in both *mdx/Pln*$^{+/+}$ and *mdx/Pln*$^{-/-}$ compared to WT mice, however, there were no differences between *mdx* groups (Fig. 3A). In DIA, there was significantly greater fibrosis in the *mdx/Pln*$^{+/+}$ ($p < 0.003$) and *mdx/Pln*$^{-/-}$ ($p < 0.02$) than WT, with no differences between *mdx* and *mdx/Pln*$^{-/-}$ (Fig. 3B).

Fibre type analysis in SOL revealed no differences in the relative quantity of type I and type IIA fibres across the three experimental groups, however, there was a shift towards type IIB in the *mdx/Pln*$^{-/-}$ SOL, as the proportion of IIB fibres was significantly greater than *mdx/Pln*$^{+/+}$ ($p < 0.009$) and WT ($p < 0.02$) (Fig. 4A and B). Additionally, there was an increase in type IIX in the *mdx/Pln*$^{-/-}$ SOL, as the proportion of these fibres was significantly greater than *mdx/Pln*$^{+/+}$ and WT ($p < 0.03$) (Fig. 4A and B). In DIA, the percentage of type IIA fibres was not different between groups, however, the proportion of type I fibres in *mdx/Pln*$^{+/+}$ ($p < 0.02$) and *mdx/Pln*$^{-/-}$ ($p < 0.008$) was significantly reduced compared to WT. Furthermore, the quantity of type IIB fibres was significantly greater in *mdx/Pln*$^{-/-}$ compared to both *mdx/Pln*$^{+/+}$ ($p < 0.03$) and WT ($p < 0.007$) and the proportion of type IIX fibres was significantly greater in *mdx/Pln*$^{-/-}$ compared to both *mdx/Pln*$^{+/+}$ ($p < 0.04$) and WT ($p < 0.01$) (Fig. 4A and C)

Cross sectional area (CSA) evaluation of SOL indicated no differences in type I and type IIA fibre size between the groups, however, the fibre size of type IIB fibres in *mdx/Pln*$^{-/-}$ was significantly greater compared to *mdx/Pln*$^{+/+}$ ($p < 0.03$) (Fig. 4A and D). The amount of type IIB fibres in WT was too low to accurately determine CSA of those fibres. There were no differences in CSA for type I, IIA and IIB fibres between experimental groups in DIA (Fig. 4A and E).

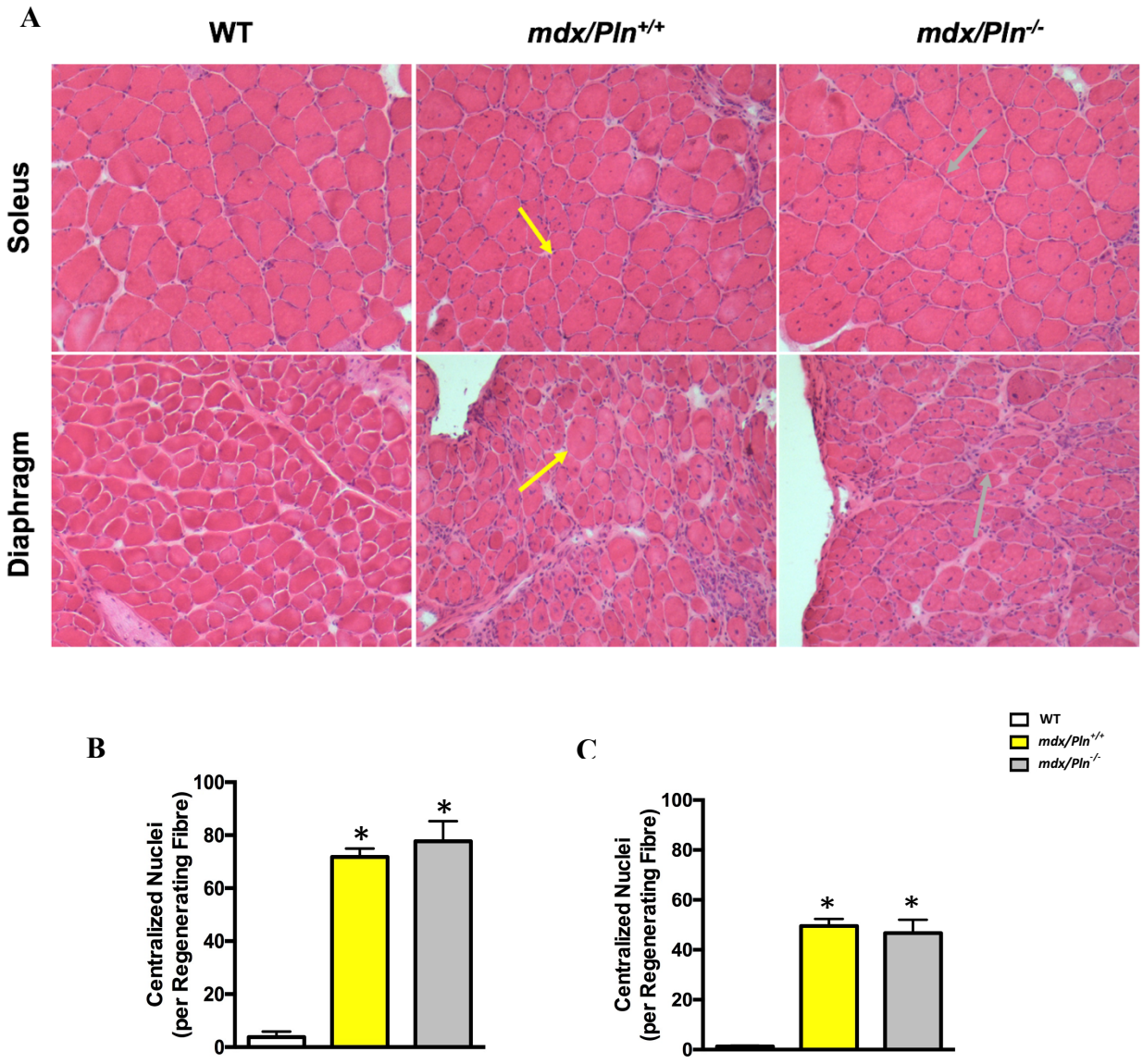

Figure 2. *Pln* deletion had no effect on central nucleation in *mdx* mice. (**A**) Representative H&E stain of soleus and diaphragm cross sections from WT (n = 6), *mdx/Pln*$^{+/+}$ (n = 6) and *mdx/Pln*$^{-/-}$ (n = 6) mice. Quantitation of the proportion of centralized nuclei in SOL (**B**) and DIA (**C**) revealing no differences in the quantities of centrally localized nuclei between *mdx* groups. * indicates a significant difference compared with WT ($p < 0.05$).

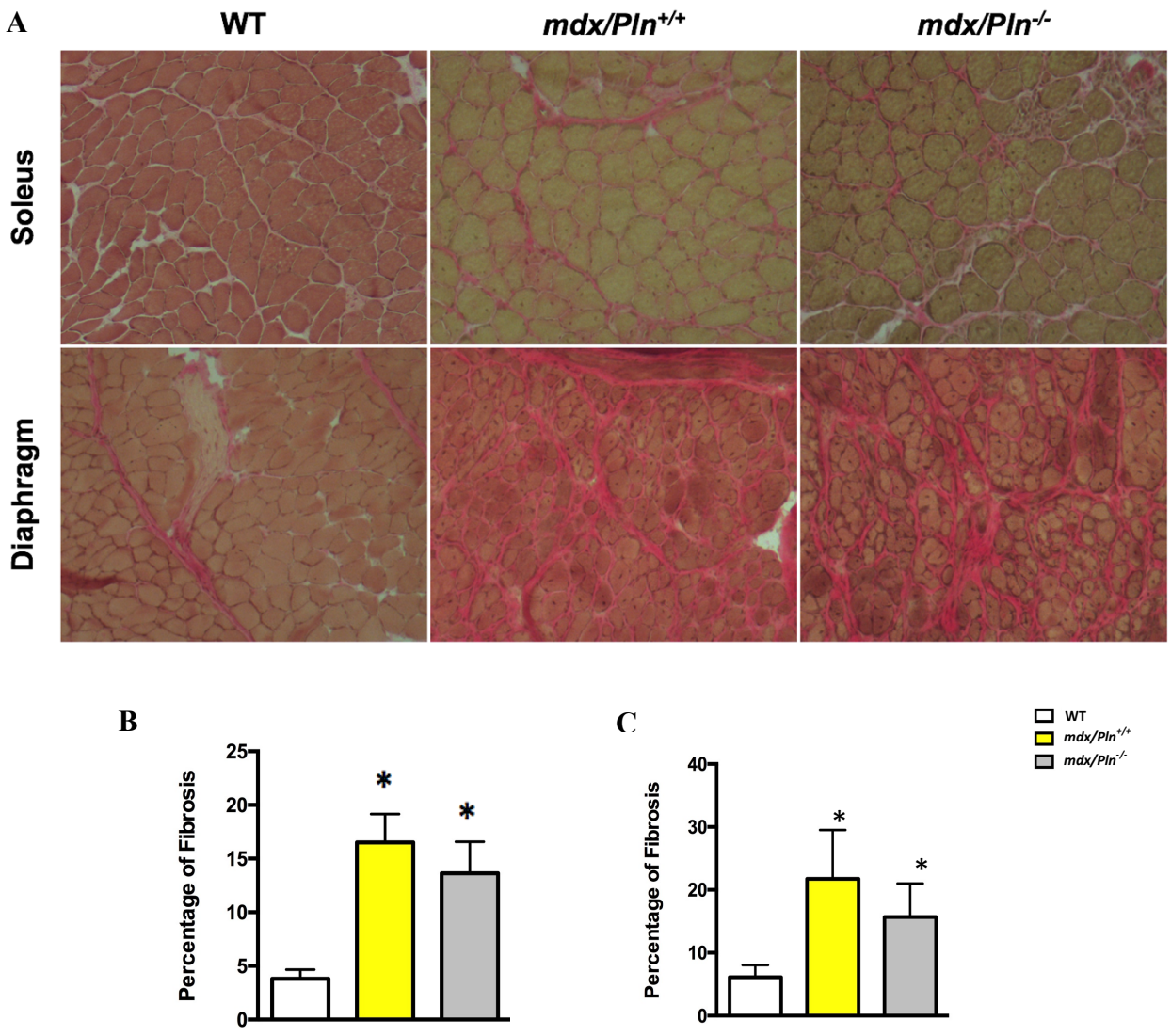

Figure 3. *Pln* ablation did not improve fibrosis in *mdx* mice.
(**A**) Representative Van Gieson stain showing fibrotic levels between WT (n = 6), *mdx/Pln*$^{+/+}$ (n = 6) and *mdx/Pln*$^{-/-}$ (n = 6) mice in the soleus and diaphragm cross sections. Quantitation of the of the level of fibrosis in both in SOL (**B**) and DIA (**C**) revealing no differences in the level of fibrosis between *mdx* groups. * indicates a significant difference compared with WT ($p < 0.05$).

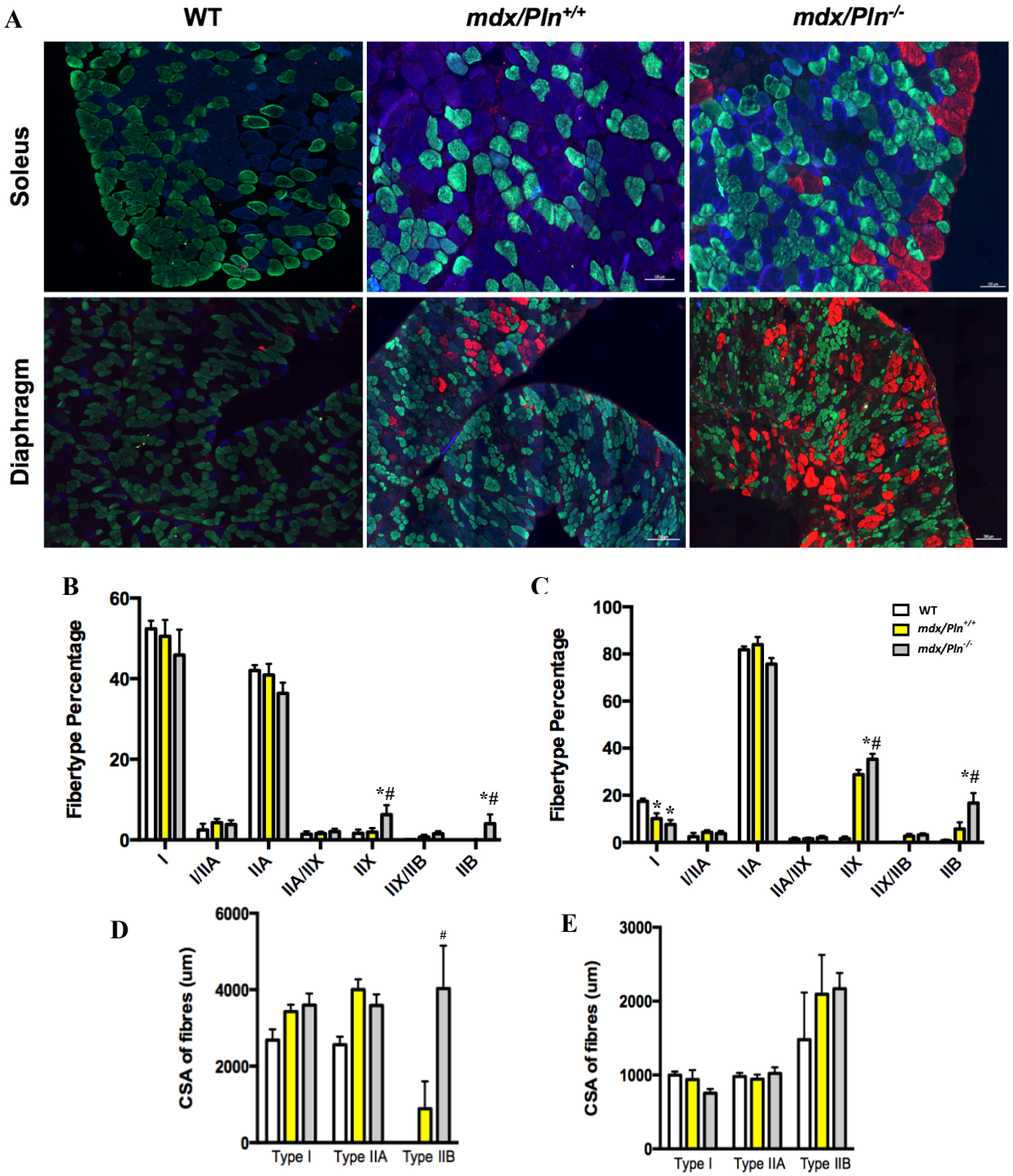

Figure 4. *Pln* deletion increased the percentage and the CSA of type IIB fibres in *mdx* mice.
(**A**) Representative immunofluorescent staining of soleus and diaphragm cross sections from WT (n = 6), *mdx/Pln*$^{+/+}$ (n = 6) and *mdx/Pln*$^{-/-}$ (n = 7) mice. Quantitation of the fibre type proportions in (**B**) SOL and (**C**) DIA revealing a fibre type shift to type IIB in *mdx/Pln*$^{-/-}$ muscles; Quantitation of the fibre type cross sectional area in (**D**) SOL and (**E**) DIA highlighting the differences in size between fibre types; * indicates a significant difference from WT ($p < 0.05$) and # indicates a significant difference from *mdx/Pln*$^{+/+}$ ($p < 0.03$).

Ca^{2+} - Handling Protein Expression

Western blotting was conducted on SOL and DIA muscle homogenates from the three experimental groups (Fig. 5). Expectedly, the expression of SLN was elevated in both *mdx* groups relative to WT ($p < 0.05$), however, SLN content was lower in *mdx/Pln*$^{-/-}$ compared to *mdx/Pln*$^{+/+}$ ($p = 0.03$) in DIA (Fig. 5B) and there was a similar trend ($p = 0.07$) in SOL (Fig. 5A). With regards to PLN expression, it was significantly higher in *mdx/Pln*$^{+/+}$ relative to WT in SOL (Fig. 6C, $p < 0.04$) but it was not different between *mdx/Pln*$^{+/+}$ and WT in DIA (Fig. 5D). PLN protein was not detected in *mdx/Pln*$^{-/-}$ muscles.

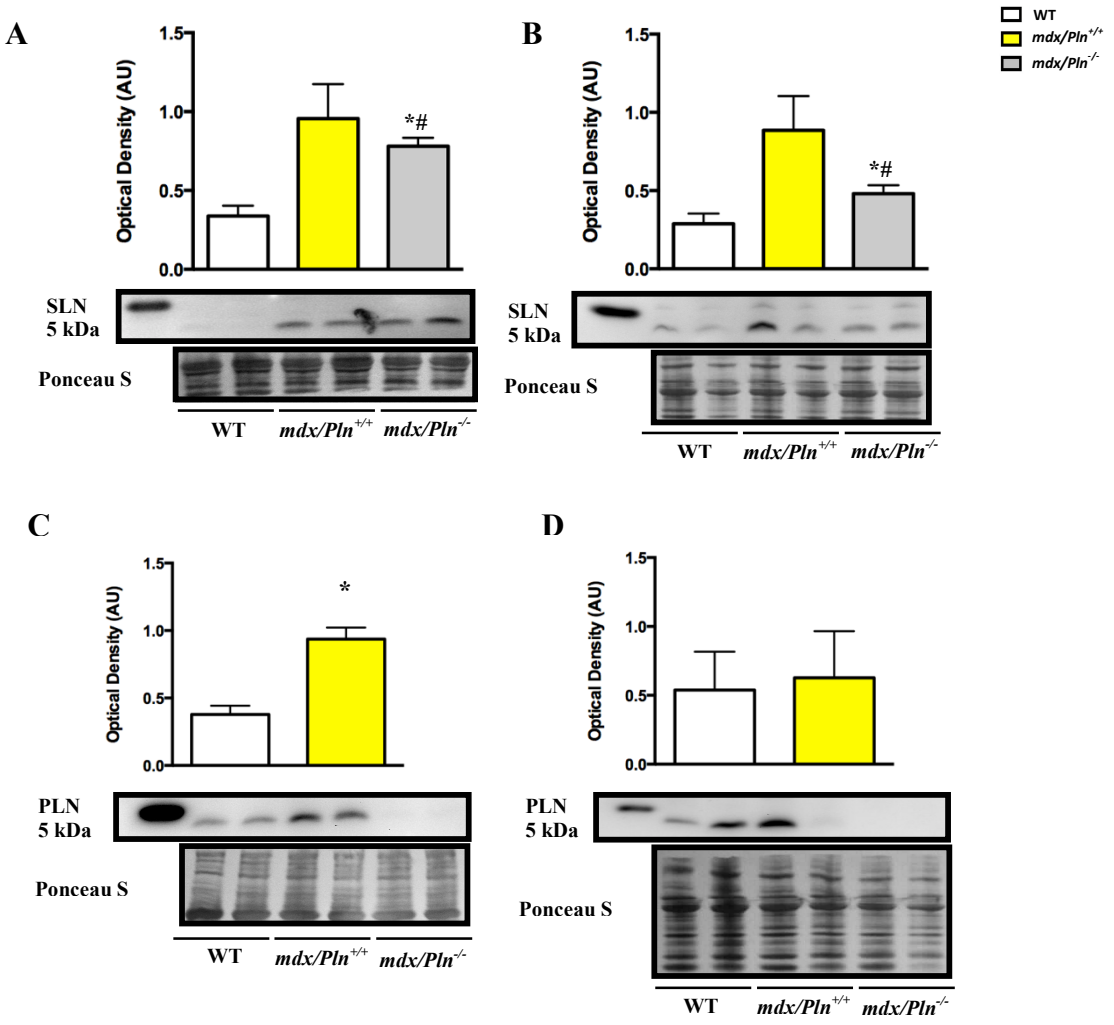

Figure 5. SLN and PLN protein expression in SOL and DIA from WT, *mdx/Pln*$^{+/+}$ and *mdx/Pln*$^{-/-}$ mice. Western blotting was performed on SOL and DIA homogenates from 4-6 month old WT, *mdx/Pln*$^{+/+}$ and *mdx/Pln*$^{-/-}$ animals. (n = 8 for each genotype). SLN content was increased in SOL (**A**) and DIA (**B**) in *mdx* groups relative to WT. PLN content in SOL (C) but not DIA (D) was higher in *mdx/Pln*$^{+/+}$ mice compared with WT. * indicates a significant difference from WT ($p < 0.05$) and # indicates a significant difference from *mdx/Pln*$^{+/+}$ ($p < 0.03$).

Skeletal Muscle Functional Assessment

Whole soleus muscles were excised from 4-6 month old WT, *mdx/Pln*$^{+/+}$, and *mdx/Pln*$^{-/-}$ mice and stimulated ex-vivo to assess isometric contractile properties (Fig. 6). The solei of *mdx/Pln*$^{+/+}$ and *mdx/Pln*$^{-/-}$ mice exhibited a significant reduction in force production compared to their WT counterparts at all frequencies, with $p = 0.001$ (Fig. 6A). Furthermore, the force generated by the *mdx/Pln*$^{-/-}$ mice was significantly decreased at all stimulation frequencies when compared to *mdx/Pln*$^{+/+}$ mice, with significance occurring at twitch ($p = 0.05$) and 30 – 50 Hz ($p < 0.05$), and trending significance at stimulation frequencies from 60 – 100 Hz ($p < 0.1$) (Fig. 6A). The rate of relaxation at each stimulation frequency was depressed for *mdx/Pln*$^{-/-}$ compared to both *mdx/Pln*$^{+/+}$ and WT groups. Significance was present at twitch, 5 and 10 Hz when comparing *mdx/Pln*$^{-/-}$ to WT ($p < 0.05$). Significance occurred at twitch, 5 and 30 Hz ($p < 0.05$) and trending significance was present at 10, 20, 40 – 70 and 90 Hz ($p < 0.1$) when comparing between *mdx* groups (Fig. 6B). The contraction rate across the three experimental groups mirrored the relaxation rate, with a significant decline that was statistically significant at all stimulation frequencies for *mdx/Pln*$^{-/-}$ compared to both *mdx/Pln*$^{+/+}$ and WT groups ($p < 0.05$) (Fig. 6C). Interestingly, there was no significant difference in both the relaxation rate and contraction rate between *mdx/Pln*$^{+/+}$ and WT.

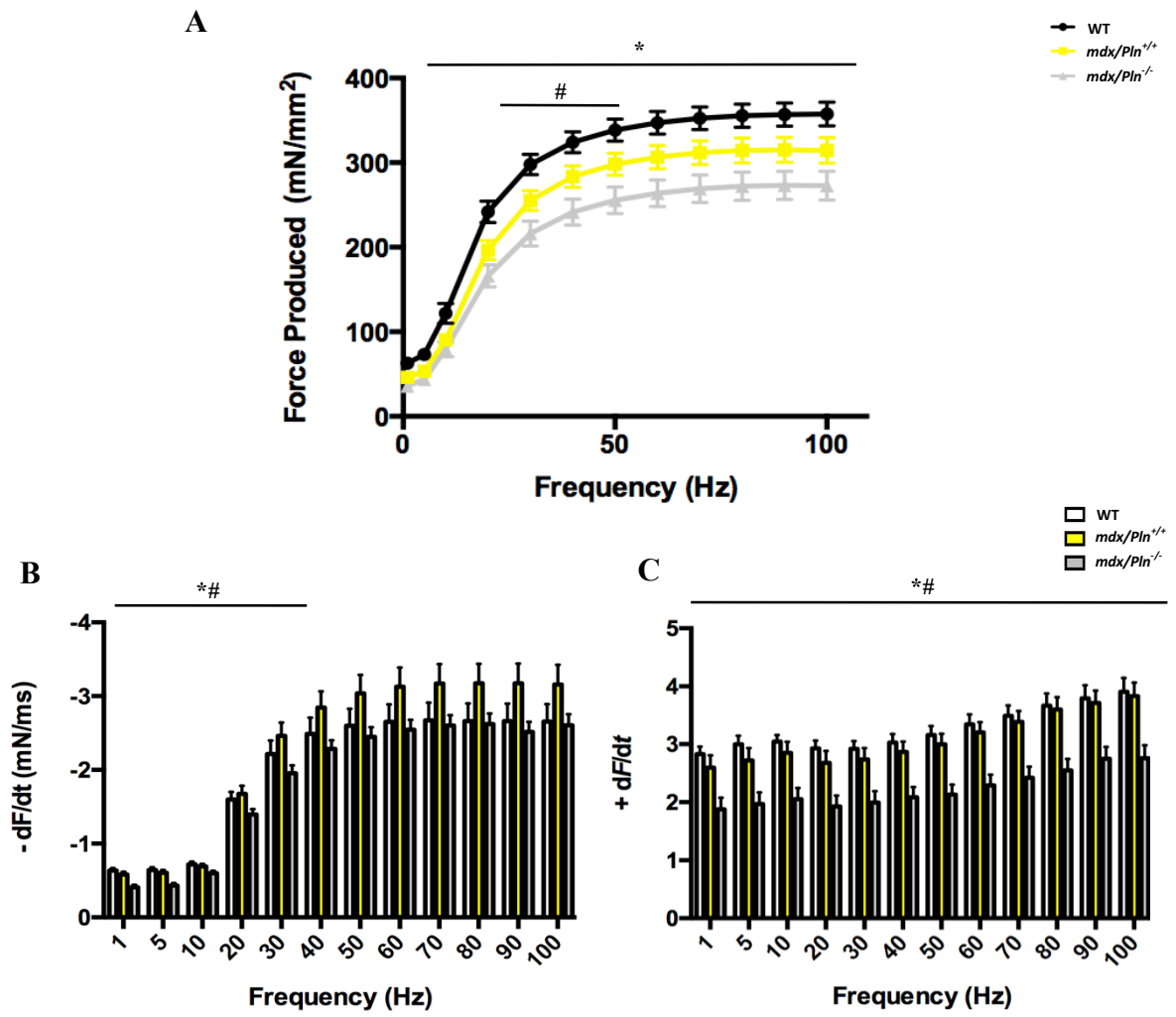

Figure 6. Force Analysis demonstrating the effect of *Pln* ablation on the *mdx* phenotype.
(A) Force frequency curves normalized to cross sectional area, demonstrating the decline in force generation observed in *mdx/Pln*$^{-/-}$ (n = 10) compared to WT (n = 11) and *mdx/Pln*$^{+/+}$ (n = 13) mice. Relaxation rates **(B)** were elevated in *mdx/Pln*$^{+/+}$ and WT compared to *mdx/Pln*$^{-/-}$. Rates of contraction **(C)** were depressed in *mdx/Pln*$^{-/-}$ mice compared to WT and *mdx/Pln*$^{+/+}$; * indicates a significant difference from WT ($p < 0.05$) and # indicates a significant difference from *mdx/Pln*$^{+/+}$ ($p < 0.05$).

SERCA Functional Assessment

SERCA functional assessment consisted of two assays: Ca^{2+} - Uptake and Ca^{2+} - ATPase activity, and was conducted on SOL and DIA homogenate. Compared with WT, Ca^{2+} uptake in SOL was lower ($p < 0.02$) in both the *mdx/Pln*$^{+/+}$ and *mdx/Pln*$^{-/-}$ groups, with significance at [Ca^{2+}] ranging from 150 nM to 1000 nM (Fig. 7). Additionally, the rate of Ca^{2+} uptake was significantly reduced for the *mdx/Pln*$^{-/-}$ group compared to *mdx/Pln*$^{+/+}$, with statistical significance evident at [Ca^{2+}] ranging from 200 nM to 1000 nM (Fig. 7, $p < 0.04$). An interesting qualitative observation is that the [Ca^{2+}] at which the rate of Ca^{2+} uptake plateaued was higher in *mdx/Pln*$^{-/-}$ SOL: Ca^{2+} uptake was evident for WT and *mdx/Pln*$^{+/+}$ homogenate at 100 nM, however, for the majority of *mdx/Pln*$^{-/-}$ tissue, Ca^{2+} uptake was undetectable below 200 nM.

Ca^{2+}-uptake assays in DIA revealed similar results as SOL. The rate of Ca^{2+}-uptake was significantly higher ($p < 0.01$) in WT compared to the two *mdx* groups, with significance at [Ca^{2+}] ranging from 100 nM to 1000 nM (Fig. 8). Moreover, the rate of Ca^{2+} uptake for the *mdx/Pln*$^{-/-}$ group was significantly depressed compared to the *mdx/Pln*$^{+/+}$ group, with significance at a [Ca^{2+}] of 250 nM ($p = 0.03$) and trending significance at [Ca^{2+}] ranging from 100 nM to 200mnM ($p < 0.1$). Once again, this rate of Ca^{2+} uptake plateaued earlier for the *mdx/Pln*$^{-/-}$ tissue compared to *mdx/Pln*$^{+/+}$ and WT.

Interestingly, while the Ca^{2+} - uptake assay revealed differences between experimental groups, the ATPase assay indicated no significant differences in either Vmax or K_{Ca} between WT, *mdx/Pln*$^{+/+}$ and *mdx/Pln*$^{-/-}$ in either the SOL (Fig. 9) or DIA (Fig. 10) muscles.

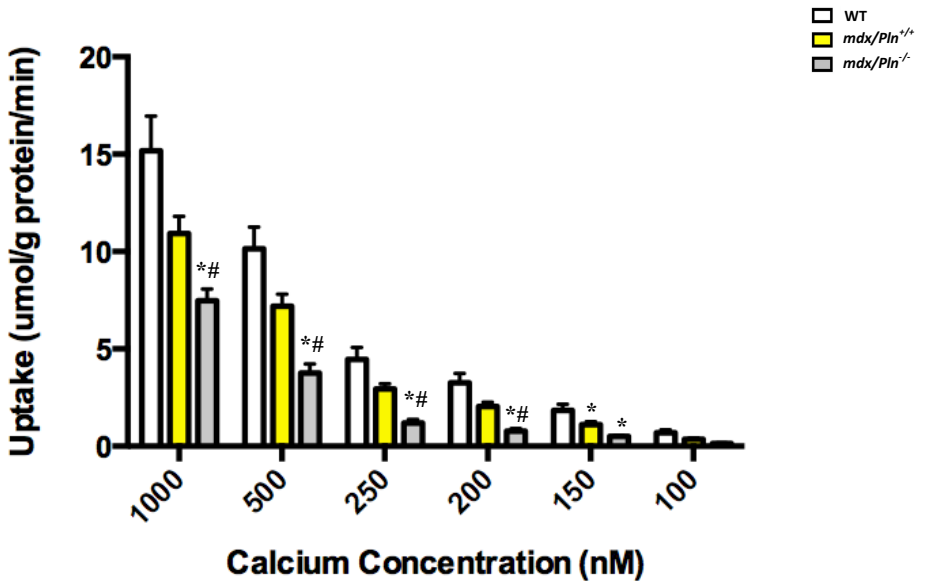

Figure 7. *Pln* deletion reduced the rate of Ca^{2+} uptake in soleus.
Ca^{2+} - Uptake was assessed on homogenates isolated from 4 – 6 month old WT (n = 9), *mdx/Pln*$^{+/+}$ (n = 7) and *mdx/Pln*$^{-/-}$ (n = 9) SOL muscles and was significantly depressed in *mdx/Pln*$^{-/-}$ compared to both WT and *mdx/Pln*$^{+/+}$ across [Ca^{2+}] ranging from 100 nM to 1000 nM; * indicates a significant difference from WT ($p < 0.05$) and # indicates a significant difference from *mdx/Pln*$^{+/+}$ ($p < 0.05$).

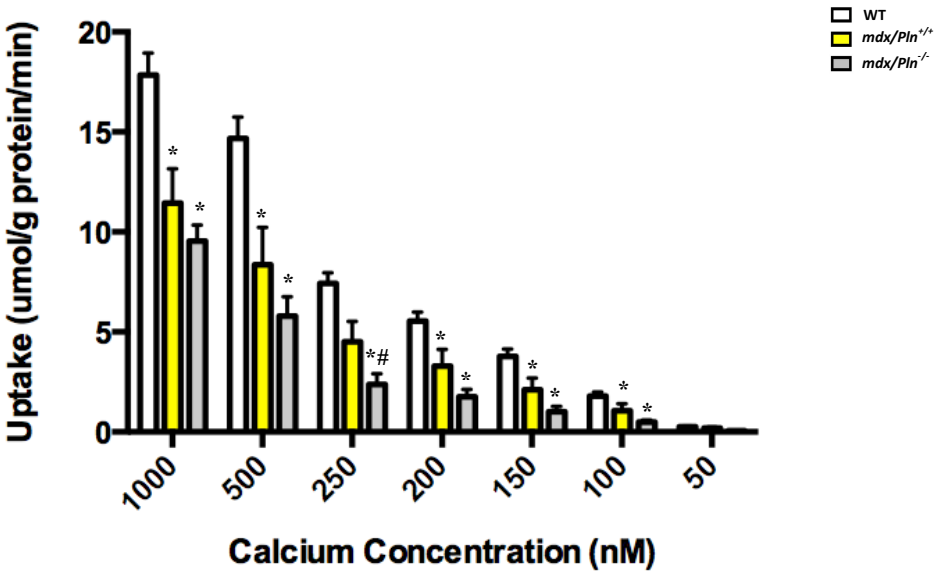

Figure 8. *Pln* deletion reduced the rate of Ca^{2+} uptake in diaphragm.
Ca^{2+} - Uptake was assessed on homogenates isolated from 4 – 6 month old WT (n = 9), *mdx/Pln*$^{+/+}$ (n = 7) and *mdx/Pln*$^{-/-}$ (n = 9) DIA muscles and was significantly depressed in *mdx/Pln*$^{-/-}$ compared to both WT and *mdx/Pln*$^{+/+}$ across [Ca^{2+}] ranging from 50 nM to 1000 nM; * indicates a significant difference from WT ($p < 0.05$) and # indicates a significant difference from *mdx/Pln*$^{+/+}$ ($p < 0.05$).

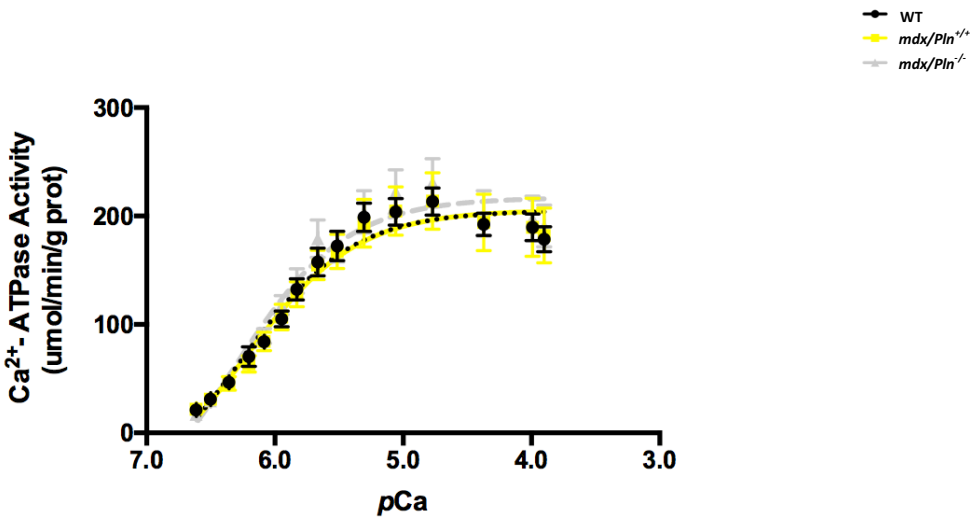

	V_{max}	K_{Ca}
WT	217.9 ± 12.3	6.30 ± 0.099
mdx	216.4 ± 25.4	6.30 ± 0.11
***mdx Pln*$^{-/-}$**	231.9 ± 21.9	6.36 ± 0.079

Figure 9. Ca^{2+} - ATPase activity is unaltered in soleus muscle
Ca^{2+} - ATPase activity was assessed on homogenates isolated from 4 – 6 month old WT, *mdx/Pln*$^{+/+}$ and *mdx/Pln*$^{-/-}$ mouse SOL muscles (n = 8 per genotype) over [Ca^{2+}] ranging from *p*Ca 7 to *p*Ca 3.5 to obtain V_{max} and K_{Ca}, and demonstrated no significant differences in these measures across the three experimental groups.

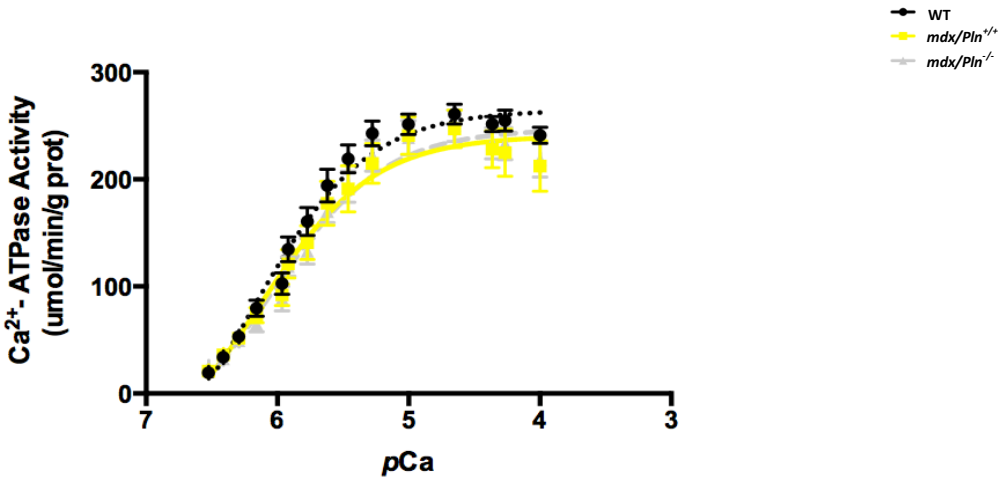

	V_{max}	K_{Ca}
WT	265.7 ± 8.8	6.19 ± 0.098
mdx	253.8 ± 17.8	6.15 ± 0.12
***mdx Pln*$^{-/-}$**	252.8 ± 15.6	6.11 ± 0.11

Figure 10. Ca^{2+} - ATPase activity is unaltered in diaphragm muscle
Ca^{2+} - ATPase activity was assessed on homogenates isolated from WT (n = 8), *mdx/Pln*$^{+/+}$ (n = 10) and *mdx/Pln*$^{-/-}$ (n = 10) mouse DIA muscles over [Ca^{2+}] ranging from *p*Ca 7 to *p*Ca 3.5 to obtain V_{max} and K_{Ca} and demonstrated no significant differences in either of these measures across the three experimental groups.

Discussion

This study aimed to characterize the role of PLN in DMD. Based on current literature and our understanding of the role of PLN in cardiac tissue, it was hypothesized that the ablation of PLN would restore SERCA activity and thus alleviate DMD pathology in *mdx* mice. Unexpectedly, PLN ablation in the *mdx* mouse model resulted in: 1) elevations in centralized nucleation; 2) a reduction in the ability to generate force; and 3) impairments in SERCA Ca^{2+} uptake when compared to *mdx/Pln*$^{+/+}$ mice. The fact that Ca^{2+} uptake was reduced in the absence of PLN is completely paradoxical to our current understanding of the role of PLN in healthy skeletal muscle and could suggest that in the context of skeletal muscle disease, the interaction between PLN and SERCA could provide protection during times of physiological stress.

Histological analysis of centralized nuclei allows for quantitation of muscle turnover, as it is a hallmark indicator of muscle degeneration/regeneration cycling. In *mdx* mice, which are characterized by progressive muscle degeneration and elevated muscle turnover rates, the amount of central nucleation was significantly elevated in both muscles compared to WT. It has been demonstrated that improved SERCA function, and thus improved Ca^{2+} - handling, ameliorates this histological marker of disease. SERCA1 overexpression profoundly reduced central nucleation in the quadriceps, SOL and DIA muscles of *mdx* mice [95]. The aim of targeting *Pln* in the *mdx* phenotype was to alleviate SERCA dysfunction, however, the opposite was observed, as *mdx/Pln*$^{-/-}$ mice exhibited the lowest rates of Ca^{2+} uptake, which was associated with a trending increase in central nucleation in SOL compared to *mdx/Pln*$^{+/+}$ mice. This result indicates that in the SOL muscle, the absence of *Pln* contributed to greater muscle wasting. However, the same cannot be inferred for DIA, as the proportion of central nucleation was not statistically different between *mdx* groups. These muscle differences indicate a dissociation

between impairments in SERCA and central nucleation since *Pln* ablation caused further impairments in SERCA function in both muscles but central nucleation wasn't affected equally in both muscles. One possible explanation for these results relates to the variability in disease manifestation and progression in different affected *mdx* muscles [70, 116]. As previously mentioned, reports from numerous studies have demonstrated that not all affected muscles in *mdx* mice are equally susceptible to muscle degeneration. Hind limb muscles undergo extensive cycles of muscle turnover and are capable of prolonged successful regeneration, whereas, the *mdx* diaphragm exhibits a greater dystrophic pattern with a reduced regenerative capacity [68, 70, 117]. The absence of *Pln* could have imposed a greater effect on SOL because of its ability to undergo successive cycles of muscle degeneration/regeneration, whereas, DIA may have reached its regenerative plateau.

It is well established that *mdx* mice undergo a fast-to-slow fibre type shift in order to delay disease progression, as slow twitch fibres show reduced susceptibility to damage due to increased utrophin expression [72]. Interestingly, *Pln* deletion in the *mdx* mouse caused an elevation in type IIB fibres in both SOL and DIA, suggesting a maladaptive response. The rise in the proportion of type IIB fibres in *mdx/Pln*$^{-/-}$ SOL relative to *mdx/Pln*$^{+/+}$ was accompanied by no change in type I fibres and a slight decrease in type IIA fibres. This transition was more robust in *mdx/Pln*$^{-/-}$ DIA, with a significant decline of type I fibres concomitant to the increase of type IIB fibres compared to *mdx/Pln*$^{+/+}$ and WT. A similar finding was reported by Fajardo *et al.* (unpublished) in a *mdx/Sln*$^{-/-}$ model, as the ablation of *Sln* in the *mdx* phenotype induced a slow-to-fast fibre type shift in both SOL and DIA [118]. This transition was attributed to a decline in calcineurin activation as a result of the absence of *Sln* signalling [118]. Calcineurin, a Ca^{2+}-calmodulin–dependent serine/threonine protein phosphatase, has been implicated in numerous

signalling pathways, however, most pertinent to the dystrophic environment is its role in promoting type I/IIA fibres and stimulating utrophin expression [72, 119, 120]. Transgenic expression of an activated form of calcineurin has been shown to mitigate the myopathy in *mdx* mice through increases type I/IIA fibres and in utrophin content [119]. In contrast, the deletion of *Sln* resulted in reductions in calcineurin activation and utrophin content, as well as an increase in type IIB fibres [118]. Though calcineurin activation and utrophin content were not measured in this study, *mdx/Pln*$^{-/-}$ mice exhibited a significant decline in *Sln* expression in both SOL and DIA, and this could corroborate *Sln*'s role in activating calcineurin based on the slow to fast fibre type transition and an overall worsening of the myopathy, consistent with the *mdx/Sln*$^{-/-}$ model. On the other hand, the ablation of SLN improved SERCA Ca^{2+} - handling in *mdx* mice, thus potentially reducing the $[Ca^{2+}]_i$ and calcineurin activation that corresponds with the fibre type transition, whereas in the *mdx/Pln*$^{-/-}$ model there was a reduction in SERCA function. As such, it would be hypothesized that with decreased SERCA Ca^{2+} - uptake, there would be an increase in $[Ca^{2+}]_i$ and this would be accompanied by greater calcineurin activation leading to greater utrophin expression and a shift to slow twitch fibres. Interestingly, the opposite was observed and it is unclear how this occurred. It should be noted that in this study, it has been assumed that the reduction in SERCA Ca^{2+} - uptake induces greater $[Ca^{2+}]_i$, however, $[Ca^{2+}]_i$, and other factors affecting cytosolic Ca^{2+} (such as RyR Ca^{2+} release, parvalbumin or mitochondrial Ca^{2+} - uptake) were not measured. As such, before conclusions can be made on the effects of PLN ablation on calcineurin signalling and fibre type in the *mdx* model, it would be imperative to measure not only SERCA activity, but the $[Ca^{2+}]_i$, calcineurin signalling, and the additional factors contributing to intracellular Ca^{2+} homeostasis. Overall, these results really highlight the interplay

between the two SERCA regulators and calls for the need to expand the understanding of both PLN and SLN in a cellular signalling context.

The force analysis results of this study were comparable to the literature. While the increase in muscle mass of *mdx/Pln*$^{+/+}$ SOL was not as pronounced compared with previous reports upon normalization of force to mass and fibre cross sectional area [79], force generation significantly declined across the range of stimulation frequencies compared with WT. The reduction in force generation in dystrophic muscle is further impaired by *Pln* deletion as *mdx/Pln*$^{-/-}$ SOL showed a significant decrease at all stimulation frequencies relative to *mdx/Pln*$^{+/+}$. This could partly be due to the slow-to-fast fibre type transition previously discussed. This myopathy is not uniform in disease progression as there is an increased susceptibility of type IIB fibres to necrosis during contraction, which may be related to a heightened vulnerability to oxidative damage [69, 102]. Dystrophic muscle, particularly type IIB fibres, exhibit increases in lipid peroxidation, oxidation of proteins and the induction of antioxidant enzymes that precede the onset of necrosis [102]. It has been well documented that contracting skeletal muscle is a major source of oxidizing free radical species and this, coupled with the already elevated levels of free radical damage in dystrophic muscle could contribute to the greater susceptibility to muscle damage and reduced force production [102, 121, 122]. It is possible that during normal ambulation, *mdx/Pln*$^{-/-}$ muscle is more susceptible to contraction induced mechanical stress. Another factor that could contribute to depressed force generation is the reduced SERCA Ca^{2+} - uptake observed in *mdx/Pln*$^{-/-}$ SOL muscle. A consequence of reduced Ca^{2+} - uptake into the SR is a smaller SR Ca^{2+} load. With a lower Ca^{2+} reserve in the SR, there is less Ca^{2+} available to be released during subsequent contractions. As such, less Ca^{2+} will be available to bind to troponin C and promote the formation of cross bridges to generate force.

Force analysis data additionally revealed impairments in the relaxation rate for *mdx/Pln*$^{-/-}$ SOL relative to WT and *mdx/Pln*$^{+/+}$. *Pln* has been demonstrated to regulate rates of relaxation and contraction, and it was expected that in its absence SERCA activity, and thus the relaxation rate, would improve [1, 2]. Moreover, as mentioned previously, the fibre type transition to fast twitch fibres observed in the *mdx/Pln*$^{-/-}$ mice could facilitate enhanced calcium clearance, as these fibres exhibit a 5-7-fold greater density of SERCA [21, 25]. This could potentially be expected counteract the impairments in SERCA function and enable faster and more efficient Ca^{2+} clearance in *mdx/Pln*$^{-/-}$ compared to WT [21, 25]. Surprisingly, the opposite was observed, in that the relaxation rate was slower, additionally, *mdx/Pln*$^{-/-}$ twitch half relaxation time is trending to be slower, than that of the WT and *mdx/Pln*$^{+/+}$ ($p = 0.065$). While unexpected, this is consistent with the overall worsening of myopathy observed in the *mdx/Pln*$^{-/-}$ mice in terms of greater centralized nuclei, slow-to-fast fibre type transition, reduced rates of Ca^{2+} uptake, and reductions in force production. The lack of a difference in the relaxation rate between WT and *mdx/Pln*$^{+/+}$ is unexpected for the *mdx/Pln*$^{+/+}$ phenotype due to the reduction in SERCA expression, as well as, the SERCA dysregulation observed in this myopathy, which would affect the clearance of Ca^{2+} from the cytosol to the SR and thus impede relaxation [112]. The drastic impairment in the contraction rate at all stimulation frequencies in *mdx/Pln*$^{-/-}$ SOL is consistent with the reduced rate of Ca^{2+} uptake and prolonged relaxation rate. As previously mentioned, a decline in Ca^{2+} - uptake into the SR results in a smaller SR Ca^{2+} load, as such, with a smaller Ca^{2+} reserve in the SR, there is less Ca^{2+} available to be released during subsequent contractions. Furthermore, though not assessed in this study, it has been reported in the literature that RyR undergoes oxidative damage in the dystrophic environment [95]. Therefore, the depression in SR

Ca^{2+} load coupled with impairments in RyR mediated Ca^{2+} release could contribute to the longer contraction rate in *mdx/Pln*$^{-/-}$ SOL.

The dissociation of *Pln* from SERCA, as mediated by conditions of high $[Ca^{2+}]_i$ or adrenergic stimulation, has been shown to enhance SERCA mediated Ca^{2+} uptake. As such, it was hypothesized that the ablation of *Pln* would allow for improved Ca^{2+} handling and alleviate the dystrophic phenotype. However, the rate of Ca^{2+} uptake was depressed in both *mdx* groups relative to WT in both muscles examined. Furthermore, ablation of *Pln* resulted in a pronounced reduction of Ca^{2+} uptake in the *mdx/Pln*$^{-/-}$ group compared to *mdx/Pln*$^{+/+}$ in both SOL and DIA. Additionally, the $[Ca^{2+}]$ at which SERCA mediated uptake plateaued was consistently higher in *mdx/Pln*$^{-/-}$ relative to *mdx/Pln*$^{+/+}$. These results may be due either to a decline in SERCA expression and/or increased SERCA susceptibility to damage in the dystrophic environment. While the expression of SERCA isoforms and their susceptibility to damage were not assessed in this thesis, analyses are currently underway to determine the effect of PLN ablation on both the expression pattern and susceptibility to oxidation and nitrosylation.

Interestingly, both muscles exhibited an increase in PLN content in *mdx/Pln*$^{+/+}$ relative to WT. The fact that PLN is upregulated in this *mdx/Pln*$^{+/+}$ model and that there is a worsening of the overall myopathy, muscle weakness and SERCA impairment in the absence of PLN suggests that PLN is required in dystrophic muscle to protect SERCA from damage. As indicated earlier, PLN interacts physically with the SERCA protein, possibly even in its phosphorylated form. Therefore, it is plausible that this interaction could provide structural and functional protection to SERCA during times of stress. Indeed, our lab has examined the interaction between SERCA and PLN when faced with heat stress and demonstrated that PLN provided protection against SERCA nitrosylation and carbonyl formation (unpublished).

It has been shown that both SERCA1 and SERCA2 are highly susceptible to damage incurred by exposure to oxidative stress, due to the considerable number of cysteine residues (24 and 26 Cys residues, respectively) which comprise the proteins [107-109]. Oxidative stress can include oxidation, nitrosylation, S –glutathiolation of protein thiols, and Tyr nitration and can structurally alter the pump to induce impairments that cannot be overcome and result in the loss of function [107-109]. Our lab and others have demonstrated that protein-protein interactions can stabilize SERCA and offer protection against the many forms of oxidative stress [107]. One such protein-protein interaction is that of the chaperone protein, heat shock protein 70 (HSP70) and SERCA [107, 110]. In examining the protective effects of HSP70 on both SERCA1a and SERCA2a isoforms, HEK – 293 cells were cotransfected with cDNA encoding human HSP70 and either rabbit SERCA1a or SERCA2a, respectfully, and exposed to 37°C and 41°C for various incubation times [107]. Co- immunopreciptation revealed a physical interaction between HSP70 and both isoforms that protected against their thermal inactivation. The protein-protein interaction maintained maximal SERCA activity and prevented SERCA nitrosylation and carbonyl formation [107].

Further supporting the notion that protein-protein interactions can offer protection, is the interaction between cardiac SERCA2a and the small ubiquitin-related modifier (SUMO) protein [123]. It has been shown that SERCA2a is SUMOylated at lysine residues 480 and 585 and that this post-translational modification is essential in maintaining SERCA2a stability and thus preserving function in both mouse and human cardiac cells [123, 124]. In fact, this interaction is of such importance that its absence has been implicated in diseased states. Heart failure is associated with a decline in both SUMO expression and SERCA SUMOylation, however, increases in SUMO expression mediated by adeno-associated-virus-mediated gene delivery,

improved SERCA2a activity and in doing so rescued cardiac function in mice with heart failure to a similar extent as SERCA2a gene delivery [123]. Considering the impairments in muscle health and function incurred in *mdx/Pln*$^{-/-}$ mice, it is reasonable to speculate that SERCA lacked the protection afforded by its interaction with PLN and thus was subjected to increased nitrosylation and dysregulation in its absence. In order to investigate this further, it would be pertinent to examine the oxidation and nitrosylation states of SERCA isoforms in this myopathy in the presence and absence of PLN.

Broadening the scope outside of solely the protection offered to SERCA, it has been established that the Na^+-K^+-ATPase is modulated in a similar fashion by which PLN regulates SERCA activity. The Na^+-K^+ ATPase is an integral membrane enzyme that transports sodium ions in exchange for potassium ions at the expense of ATP hydrolysis [125, 126]. SERCA and the Na^+-K^+ ATPase share extensive structural homology, as both are members of the II class of P – type ATPases and share ~65% protein sequence similarity [126]. The γ subunit of this enzyme is a 7-kDa single-span membrane protein that physically interacts with the transmembrane region of the Na^+-K^+ ATPase in order to regulate its kinetic propertie [125, 126]. This regulatory role is carried out by direct or allosteric modification of the external cation-binding sites, thus altering the apparent affinity for Na^+ and, to a lesser extent, for K^+ [125]. Recently, it has been revealed that the absence of the γ subunit renders the Na^+-K^+ ATPase susceptible to thermal instability. Cells lacking the γ subunit demonstrated increased sensitivity to heat stress at both 41°C and 37°C, as evident by Na^+-K^+ ATPase denaturation [125]. Additionally, it has been observed that several cell lines counteract stressful conditions, such as heat shock, by upregulating γ subunit expression in order to stabilize the enzyme complex and prolong cell vitality [125]. The resemblance between the two transport proteins and their associated regulators could potentially

offer support for the notion that PLN protects SERCA in a similar fashion by which the γ subunit affords the Na^+-K^+ ATPase protection.

Lastly, the Ca^{2+} - ATPase assay revealed no differences in maximal SERCA activity nor K_{Ca} (the [Ca^{2+}] required to attain the half-maximal Ca^{2+}-ATPase activity rate) between experimental groups in both muscles. This result is very intriguing, especially in view of the stark differences in Ca^{2+} uptake rates between groups. The fact that *mdx/Pln*$^{-/-}$ SOL and DIA experienced a drastic impairment in Ca^{2+} uptake without an accompanying change in ATPase activity, indicates that Ca^{2+} uptake and ATP hydrolysis of the pumps has become severely uncoupled. Based on the three sites of physical interaction between PLN and SERCA, it would be expected that the transmembrane domain, which houses the Ca^{2+} binding domain, but not the ATP binding domain, would be afforded protection by the presence of PLN. Therefore, with PLN ablation, the Ca^{2+} binding domain becomes vulnerable to damage resulting in impairments in Ca^{2+} uptake, whereas, the ATP binding domain, and thus ATP binding and hydrolysis by the pump, is unaffected.

Future Directions and Conclusions

This study highlighted the complex interaction between PLN and SERCA. It was hypothesized that the removal of PLN and thus the removal of PLN's inhibition of SERCA activity, would act to increase Ca^{2+} - uptake into the SR and remedy the aberrant Ca^{2+} signalling observed in the DMD myopathy. Unexpectedly, however, the removal of PLN further impeded SERCA mediated Ca^{2+} uptake, resulting in increases in centralized nuclei (a histological marker of muscle turnover) and reductions in force generation. One possibility that could explain these results is that the interaction between PLN and SERCA might afford the pump protection against oxidative damage. However, in order to conclusively establish the protective role of PLN, further investigations must be made. The extent of SERCA damage in the presence and absence of PLN must be determined, which can be accomplished with a co-immunopreciptation blot assessing SERCA nitrosylation in *mdx/Pln*$^{+/+}$ and *mdx/Pln*$^{-/-}$ tissue. It would also be useful to assess the pentamer to monomer ratio in these tissues, to determine if the upregulation of PLN is occurring in a manner that can bind to SERCA and offer protection (the monomeric form) or if the monomers are oligomerizing into the pentameric form and exerting a role that has not yet been evaluated.

Additionally, it would be of use to assess ROS – mediated SERCA damage in HEK – 293 cells in order to supplement the previous research conducted on thermal inactivation of SERCA in the presence and absence of PLN and SLN. A potential research design would include transfecting HEK – 293 cells with cDNA encoding WT SERCA2a alone or co-transfection with with cDNAs encoding WT SERCA2a and rabbit WT PLN or the strong or weak SERCA binding PLN mutants (I40A and N34A, respectively) [107]. Furthermore, these proteins can be linked to fluorescent tags, for instance, SERCA2a can be tagged with green fluorescent protein (GFP) and

the different PLN mutants can be tagged with yellow fluorescent protein (YFP) or red fluorescent protein (RFP). It would then be possible to observe the co-localization of these proteins, as indicative of their interaction, and it the extent of this co-localization could be quantified depending on the conditions. These cells would then be exposed to the mitochondrial un-coupler carbonyl cyanide m-chlorophenyl hydrazone (CCCP), a chemical inhibitor of oxidative phosphorylation which induces ROS production [127]. The extent of the interaction between PLN and SERCA could be determined based on the co-localization of the fluorescent tags. Additionally, the degree of ROS damage can then be confirmed based on carbonyl formation and tyrosine nitration in SERCA2a, respectively, via co-immunoprecipitation western blots, as well as, damage can be examined by Ca^{2+} - dependent SERCA2a activity. Based on the results from this thesis and on the experiments previously conducted regarding heat stress and PLN facilitated SERCA protection, it would be hypothesized that transfection of cDNA encoding WT PLN and the strong binding PLN mutant I40A would prevent oxidative damage. This protection would be expected to be accompanied by greater co-localization, reductions in carbonyl formation and tyrosine formation, and the maintenance of SERCA2a activity. However, SERCA2a transfection alone and the weak binding PLN mutant N34A would not be sufficient to counteract the damage.

It has been well documented that PLN is a component of a multimeric complex in cardiac tissue, interacting with proteins including protein phosphatase 1 (PP1), HSP20 and HAX-1, and that this complex exerts an effect on both SERCA and Ca^{2+} homeostasis [36, 128]. It could very well be the case that PLN is involved in a similar complex in skeletal muscle as well, and that the absence of PLN is affecting the expression and function of the proteins it associates with. This highlights the fact that we need to expand our understanding of PLN and SLN beyond their role

as SERCA regulators. It would be imperative to investigate the factors regulating both PLN and SLN expression, as well as, the proteins and pathways that are influenced by said expression. As speculated by Fajardo *et al* (unpublished), regulation of SLN expression could be occurring via a Ca^{2+} dependent positive feedback mechanism which involves calcineurin, NFAT and the transcription factor myocyte enhancer factor 2 (MEF2) [118]. The proposed mechanism hypothesizes that an elevation in $[Ca^{2+}]_i$ activates calcineurin and enables the dephosphorylation of NFAT (to induce translocation into the nucleus), as well as, dephosphorylation of nuclear MEF2 [118]. Activation of MEF2 and NFAT acts to promotes *Sln* transcription and consequently the SLN protein interacts with SERCA to inhibit its function and maintain the higher level of $[Ca^{2+}]_i$ [118]. The mechanism regulating PLN expression is unknown, however, investigating the regulation of protein expression and the subsequent proteins and pathways of interaction represent crucial research questions that must be addressed. Future studies can focus on skeletal muscle tissue from $Pln^{+/+}$ vs $Pln^{-/-}$ and $Sln^{+/+}$ vs $Sln^{-/-}$ mice, primarily soleus muscle as it contains elevated levels of both proteins, can be removed and homogenized. From these homogenate samples, RNA can be extracted and used for a DNA microarray, in order to establish the expression pattern of a large number of transcription factors and to determine the transcription factors that are up or down regulated in the presence and absence of PLN or SLN. Identification of these transcription factors will allow for manipulation of their expression (either knock out or overexpression) to examine the subsequent effect on PLN or SLN gene expression. Moreover, future investigations can examine fluorescently tagged proteins with optical microscopes to monitor dynamic events and interactions in living cells, such as COS – 1 or HEK – 293 cells. PLN or SLN, respectively, and the proteins they are hypothesized to interact with, can be associated with fluorescent tags and the potential interactions can be evaluated via

fluorescence resonance energy transfer (FRET) or single molecule tracking (SMT) [129]. FRET allows for a determination of the distance between two fluorophore-tagged proteins, therefore, enabling researchers to understand if and how these two proteins interact in living cells [129]. Similarly, SMT can be used to directly observe the molecular behavior of fluorophore-tagged proteins in living cells, including the way in which these proteins interact, with high temporal and spatial resolution [130]. Understanding the mechanisms regulating PLN and SLN expression, as well as the protein interactions and cell signalling pathways that these proteins contribute to under healthy conditions, will be imperative for discerning the role of these proteins in pathological conditions.

A crucial limitation to this study is that cytosolic $[Ca^{2+}]_i$ levels were not evaluated, therefore, while there was an observed reduction in SERCA mediated Ca^{2+} uptake from the cytosol, it cannot be assumed that this resulted in an overall increase in $[Ca^{2+}]_i$. Contributions from other sarcolemmal proteins, cytoplasmic buffers and mitochondria in the maintenance Ca^{2+} homeostasis were not assessed and neither were the mediators of the Ca^{2+} dysregulation pathways, such as proteolytic calpains and caspases. While this thesis focused primarily on the role of PLN and its interaction with SERCA in Ca^{2+} - homeostasis, it would certainly be beneficial to examine other critical Ca^{2+} - handling proteins to provide a comprehensive investigation of the myopathy. However, given the scope, this thesis provided valuable insights into the dystrophic environment and the protein – protein interactions regulating Ca^{2+} - homeostasis.

References

1. Slack, J.P., et al., *Phospholamban ablation enhances relaxation in the murine soleus.* Am J Physiol, 1997. **273**(1 Pt 1): p. C1-6.
2. Wolska, B.M., et al., *Effect of ablation of phospholamban on dynamics of cardiac myocyte contraction and intracellular Ca2+.* Am J Physiol, 1996. **271**(1 Pt 1): p. C391-7.
3. Pattison, J.S., et al., *Phospholamban overexpression in transgenic rabbits.* Transgenic Res, 2008. **17**(2): p. 157-70.
4. Haghighi, K., et al., *Superinhibition of sarcoplasmic reticulum function by phospholamban induces cardiac contractile failure.* J Biol Chem, 2001. **276**(26): p. 24145-52.
5. Neumann, J., et al., *Targeted overexpression of phospholamban to mouse atrium depresses Ca2+ transport and contractility.* J Mol Cell Cardiol, 1998. **30**(10): p. 1991-2002.
6. Fajardo, V.A., et al., *Phospholamban overexpression in mice causes a centronuclear myopathy-like phenotype.* Dis Model Mech, 2015. **8**(8): p. 999-1009.
7. Sarma, S., et al., *Genetic inhibition of PKA phosphorylation of RyR2 prevents dystrophic cardiomyopathy.* Proc Natl Acad Sci U S A, 2010. **107**(29): p. 13165-70.
8. Williams, I.A. and D.G. Allen, *Intracellular calcium handling in ventricular myocytes from mdx mice.* Am J Physiol Heart Circ Physiol, 2007. **292**(2): p. H846-55.
9. Hoshijima, M., *Models of dilated cardiomyopathy in small animals and novel positive inotropic therapies.* Ann N Y Acad Sci, 2004. **1015**: p. 320-31.
10. Fajardo, V.A., et al., *Co-expression of SERCA isoforms, phospholamban and sarcolipin in human skeletal muscle fibers.* PLoS One, 2013. **8**(12): p. e84304.
11. Berridge, M.J., P. Lipp, and M.D. Bootman, *The versatility and universality of calcium signalling.* Nat Rev Mol Cell Biol, 2000. **1**(1): p. 11-21.
12. Clapham, D.E., *Calcium signaling.* Cell, 2007. **131**(6): p. 1047-58.
13. Brini, M., et al., *Calcium in health and disease.* Met Ions Life Sci, 2013. **13**: p. 81-137.
14. Rossi, A.E. and R.T. Dirksen, *Sarcoplasmic reticulum: the dynamic calcium governor of muscle.* Muscle Nerve, 2006. **33**(6): p. 715-31.
15. Periasamy, M. and A. Kalyanasundaram, *SERCA pump isoforms: their role in calcium transport and disease.* Muscle Nerve, 2007. **35**(4): p. 430-42.
16. Mekahli, D., et al., *Endoplasmic-reticulum calcium depletion and disease.* Cold Spring Harb Perspect Biol, 2011. **3**(6).
17. Berchtold, M.W., H. Brinkmeier, and M. Muntener, *Calcium ion in skeletal muscle: its crucial role for muscle function, plasticity, and disease.* Physiol Rev, 2000. **80**(3): p. 1215-65.
18. Calderon, J.C., P. Bolanos, and C. Caputo, *The excitation-contraction coupling mechanism in skeletal muscle.* Biophys Rev, 2014. **6**(1): p. 133-160.
19. Fryer, M.W. and D.G. Stephenson, *Total and sarcoplasmic reticulum calcium contents of skinned fibres from rat skeletal muscle.* J Physiol, 1996. **493 (Pt 2)**: p. 357-70.
20. Inesi, G. and L. de Meis, *Regulation of steady state filling in sarcoplasmic reticulum. Roles of back-inhibition, leakage, and slippage of the calcium pump.* J Biol Chem, 1989. **264**(10): p. 5929-36.

21. Reggiani, C. and T. te Kronnie, *RyR isoforms and fibre type-specific expression of proteins controlling intracellular calcium concentration in skeletal muscles.* J Muscle Res Cell Motil, 2006. **27**(5-7): p. 327-35.
22. Gailly, P., et al., *Critical evaluation of cytosolic calcium determination in resting muscle fibres from normal and dystrophic (mdx) mice.* Cell Calcium, 1993. **14**(6): p. 473-83.
23. Carroll, S.L., M.G. Klein, and M.F. Schneider, *Decay of calcium transients after electrical stimulation in rat fast- and slow-twitch skeletal muscle fibres.* J Physiol, 1997. **501 (Pt 3)**: p. 573-88.
24. Renganathan, M., M.L. Messi, and O. Delbono, *Overexpression of IGF-1 exclusively in skeletal muscle prevents age-related decline in the number of dihydropyridine receptors.* J Biol Chem, 1998. **273**(44): p. 28845-51.
25. Leberer, E. and D. Pette, *Immunochemical quantification of sarcoplasmic reticulum Ca-ATPase, of calsequestrin and of parvalbumin in rabbit skeletal muscles of defined fiber composition.* Eur J Biochem, 1986. **156**(3): p. 489-96.
26. Leberer, E., K.T. Hartner, and D. Pette, *Postnatal development of Ca2+-sequestration by the sarcoplasmic reticulum of fast and slow muscles in normal and dystrophic mice.* Eur J Biochem, 1988. **174**(2): p. 247-53.
27. Shaikh, S.A., S.K. Sahoo, and M. Periasamy, *Phospholamban and sarcolipin: Are they functionally redundant or distinct regulators of the Sarco(Endo)Plasmic Reticulum Calcium ATPase?* Journal of Molecular and Cellular Cardiology, 2016. **91**: p. 81-91.
28. Gamu, D., et al., *Sarcolipin provides a novel muscle-based mechanism for adaptive thermogenesis.* Exerc Sport Sci Rev, 2014. **42**(3): p. 136-42.
29. Clarke, D.M., et al., *Location of high affinity Ca2+-binding sites within the predicted transmembrane domain of the sarcoplasmic reticulum Ca2+-ATPase.* Nature, 1989. **339**(6224): p. 476-8.
30. Chemaly, E.R., Bobe, R., Adnot, S., Hajjar, R. J., & Lipskaia, L. , *Sarco (Endo) Plasmic Reticulum Calcium ATPases (SERCA) Isoforms in the Normal and Diseased Cardiac, Vascular and Skeletal muscle.* . Journal of Cardiovascular Diseases & Diagnosis, 2013. **1**(113): p. 2.
31. Tupling, A.R., *The sarcoplasmic reticulum in muscle fatigue and disease: role of the sarco (endo) plasmic reticulum Ca2+-ATPase.* Canadian Journal of Applied Physiology, 2004. **29**(3): p. 308-329.
32. Lee, A.G., *Ca2+ -ATPase structure in the E1 and E2 conformations: mechanism, helix-helix and helix-lipid interactions.* Biochim Biophys Acta, 2002. **1565**(2): p. 246-66.
33. Asahi, M., et al., *Sarcolipin regulates sarco(endo)plasmic reticulum Ca2+-ATPase (SERCA) by binding to transmembrane helices alone or in association with phospholamban.* Proceedings of the National Academy of Sciences, 2003. **100**(9): p. 5040-5045.
34. Gorski, P.A., et al., *Sarco (endo) plasmic reticulum calcium ATPase (SERCA) inhibition by sarcolipin is encoded in its luminal tail.* Journal of Biological Chemistry, 2013. **288**(12): p. 8456-8467.
35. Toyofuku, T., et al., *Identification of regions in the Ca(2+)-ATPase of sarcoplasmic reticulum that affect functional association with phospholamban.* J Biol Chem, 1993. **268**(4): p. 2809-15.
36. MacLennan, D.H. and E.G. Kranias, *Phospholamban: a crucial regulator of cardiac contractility.* Nat Rev Mol Cell Biol, 2003. **4**(7): p. 566-77.

37. Akin, B.L. and L.R. Jones, *Characterizing phospholamban to sarco(endo)plasmic reticulum Ca2+-ATPase 2a (SERCA2a) protein binding interactions in human cardiac sarcoplasmic reticulum vesicles using chemical cross-linking.* J Biol Chem, 2012. **287**(10): p. 7582-93.
38. MacLennan, D.H., M. Asahi, and A.R. Tupling, *The regulation of SERCA-type pumps by phospholamban and sarcolipin.* Ann N Y Acad Sci, 2003. **986**: p. 472-80.
39. Toyoshima, C., et al., *Modeling of the inhibitory interaction of phospholamban with the Ca2+ ATPase.* Proc Natl Acad Sci U S A, 2003. **100**(2): p. 467-72.
40. Traaseth, N.J., et al., *Structural and dynamic basis of phospholamban and sarcolipin inhibition of Ca(2+)-ATPase.* Biochemistry, 2008. **47**(1): p. 3-13.
41. Gustavsson, M., et al., *Allosteric regulation of SERCA by phosphorylation-mediated conformational shift of phospholamban.* Proc Natl Acad Sci U S A, 2013. **110**(43): p. 17338-43.
42. Asahi, M., et al., *Physical interactions between phospholamban and sarco(endo)plasmic reticulum Ca2+-ATPases are dissociated by elevated Ca2+, but not by phospholamban phosphorylation, vanadate, or thapsigargin, and are enhanced by ATP.* J Biol Chem, 2000. **275**(20): p. 15034-8.
43. Jones, L.R., R.L. Cornea, and Z. Chen, *Close proximity between residue 30 of phospholamban and cysteine 318 of the cardiac Ca2+ pump revealed by intermolecular thiol cross-linking.* J Biol Chem, 2002. **277**(31): p. 28319-29.
44. James, P., et al., *Nature and site of phospholamban regulation of the Ca2+ pump of sarcoplasmic reticulum.* Nature, 1989. **342**(6245): p. 90-2.
45. Bidwell, P., et al., *Phospholamban binds with differential affinity to calcium pump conformers.* J Biol Chem, 2011. **286**(40): p. 35044-50.
46. Mueller, B., et al., *Direct detection of phospholamban and sarcoplasmic reticulum Ca-ATPase interaction in membranes using fluorescence resonance energy transfer.* Biochemistry, 2004. **43**(27): p. 8754-65.
47. Li, J., D.J. Bigelow, and T.C. Squier, *Conformational changes within the cytosolic portion of phospholamban upon release of Ca-ATPase inhibition.* Biochemistry, 2004. **43**(13): p. 3870-9.
48. Vangheluwe, P., et al., *Sarcolipin and phospholamban mRNA and protein expression in cardiac and skeletal muscle of different species.* Biochem J, 2005. **389**(Pt 1): p. 151-9.
49. Kranias, E.G. and R.J. Hajjar, *Modulation of cardiac contractility by the phospholamban/SERCA2a regulatome.* Circ Res, 2012. **110**(12): p. 1646-60.
50. Bluhm, W.F., et al., *Phospholamban: a major determinant of the cardiac force-frequency relationship.* Am J Physiol Heart Circ Physiol, 2000. **278**(1): p. H249-55.
51. Haghighi, K., et al., *Human phospholamban null results in lethal dilated cardiomyopathy revealing a critical difference between mouse and human.* J Clin Invest, 2003. **111**(6): p. 869-76.
52. Hoshijima, M., et al., *Chronic suppression of heart-failure progression by a pseudophosphorylated mutant of phospholamban via in vivo cardiac rAAV gene delivery.* Nat Med, 2002. **8**(8): p. 864-71.
53. Schmitt, J.P., et al., *Dilated cardiomyopathy and heart failure caused by a mutation in phospholamban.* Science, 2003. **299**(5611): p. 1410-3.
54. James, J., et al., *Transgenic rabbits expressing mutant essential light chain do not develop hypertrophic cardiomyopathy.* J Mol Cell Cardiol, 2002. **34**(7): p. 873-82.

55. Bers, D.M., *Cardiac excitation-contraction coupling.* Nature, 2002. **415**(6868): p. 198-205.
56. Li, L., et al., *Cardiac myocyte calcium transport in phospholamban knockout mouse: relaxation and endogenous CaMKII effects.* Am J Physiol, 1998. **274**(4 Pt 2): p. H1335-47.
57. Hove-Madsen, L. and D.M. Bers, *Sarcoplasmic reticulum Ca2+ uptake and thapsigargin sensitivity in permeabilized rabbit and rat ventricular myocytes.* Circ Res, 1993. **73**(5): p. 820-8.
58. Mercuri, E. and F. Muntoni, *Muscular dystrophies.* Lancet, 2013. **381**(9869): p. 845-60.
59. Cooper, S.T. and S.I. Head, *Membrane Injury and Repair in the Muscular Dystrophies.* Neuroscientist, 2015. **21**(6): p. 653-68.
60. Whitehead, N.P., E.W. Yeung, and D.G. Allen, *Muscle damage in mdx (dystrophic) mice: role of calcium and reactive oxygen species.* Clin Exp Pharmacol Physiol, 2006. **33**(7): p. 657-62.
61. Allen, D.G., et al., *Calcium and the damage pathways in muscular dystrophy.* Can J Physiol Pharmacol, 2010. **88**(2): p. 83-91.
62. Allen, D.G., N.P. Whitehead, and S.C. Froehner, *Absence of Dystrophin Disrupts Skeletal Muscle Signaling: Roles of Ca2+, Reactive Oxygen Species, and Nitric Oxide in the Development of Muscular Dystrophy.* Physiol Rev, 2016. **96**(1): p. 253-305.
63. McDonald, A.A., et al., *Disease course in mdx:utrophin+/- mice: comparison of three mouse models of Duchenne muscular dystrophy.* Physiol Rep, 2015. **3**(4).
64. Bulfield, G., et al., *X chromosome-linked muscular dystrophy (mdx) in the mouse.* Proc Natl Acad Sci U S A, 1984. **81**(4): p. 1189-92.
65. Sicinski, P., et al., *The molecular basis of muscular dystrophy in the mdx mouse: a point mutation.* Science, 1989. **244**(4912): p. 1578-80.
66. DiMario, J.X., A. Uzman, and R.C. Strohman, *Fiber regeneration is not persistent in dystrophic (MDX) mouse skeletal muscle.* Dev Biol, 1991. **148**(1): p. 314-21.
67. Carnwath, J.W. and D.M. Shotton, *Muscular dystrophy in the mdx mouse: histopathology of the soleus and extensor digitorum longus muscles.* J Neurol Sci, 1987. **80**(1): p. 39-54.
68. Stedman, H.H., et al., *The mdx mouse diaphragm reproduces the degenerative changes of Duchenne muscular dystrophy.* Nature, 1991. **352**(6335): p. 536-9.
69. Webster, C., et al., *Fast muscle fibers are preferentially affected in Duchenne muscular dystrophy.* Cell, 1988. **52**(4): p. 503-13.
70. Hnia, K., et al., *Pathological pattern of Mdx mice diaphragm correlates with gradual expression of the short utrophin isoform Up71.* Biochim Biophys Acta, 2006. **1762**(3): p. 362-72.
71. Selsby, J.T., et al., *Rescue of dystrophic skeletal muscle by PGC-1alpha involves a fast to slow fiber type shift in the mdx mouse.* PLoS One, 2012. **7**(1): p. e30063.
72. Chakkalakal, J.V., et al., *Expression of utrophin A mRNA correlates with the oxidative capacity of skeletal muscle fiber types and is regulated by calcineurin/NFAT signaling.* Proc Natl Acad Sci U S A, 2003. **100**(13): p. 7791-6.
73. Rafael, J.A., et al., *Skeletal muscle-specific expression of a utrophin transgene rescues utrophin-dystrophin deficient mice.* Nat Genet, 1998. **19**(1): p. 79-82.
74. Tinsley, J., et al., *Expression of full-length utrophin prevents muscular dystrophy in mdx mice.* Nat Med, 1998. **4**(12): p. 1441-4.

75. Tinsley, J.M., et al., *Amelioration of the dystrophic phenotype of mdx mice using a truncated utrophin transgene.* Nature, 1996. **384**(6607): p. 349-53.
76. Cerletti, M., et al., *Dystrophic phenotype of canine X-linked muscular dystrophy is mitigated by adenovirus-mediated utrophin gene transfer.* Gene Ther, 2003. **10**(9): p. 750-7.
77. Coulton, G.R., et al., *The mdx mouse skeletal muscle myopathy: II. Contractile properties.* Neuropathol Appl Neurobiol, 1988. **14**(4): p. 299-314.
78. Gillis, J.M., *Understanding dystrophinopathies: an inventory of the structural and functional consequences of the absence of dystrophin in muscles of the mdx mouse.* J Muscle Res Cell Motil, 1999. **20**(7): p. 605-25.
79. Lynch, G.S., et al., *Force and power output of fast and slow skeletal muscles from mdx mice 6-28 months old.* J Physiol, 2001. **535**(Pt 2): p. 591-600.
80. Zhou, L., et al., *Haploinsufficiency of utrophin gene worsens skeletal muscle inflammation and fibrosis in mdx mice.* J Neurol Sci, 2008. **264**(1-2): p. 106-11.
81. Huang, P., et al., *Impaired respiratory function in mdx and mdx/utrn(+/-) mice.* Muscle Nerve, 2011. **43**(2): p. 263-7.
82. Hopf, F.W., P.R. Turner, and R.A. Steinhardt, *Calcium misregulation and the pathogenesis of muscular dystrophy.* Subcell Biochem, 2007. **45**: p. 429-64.
83. Ohlendieck, K.C., K. P. , *Dystrophin-Associated Proteins are Greatly Reduced in Skeletal Muscle from mdx Mice. .* The Journal of Cell Biology,, 1991. **115**((6):): p. 1685-1694.
84. Dimple Bansal, K.M., Steven S. Vogel, Se´verine Groh, Chien-Chang Chen, Roger Williamson, Paul L. McNeil, Kevin P. Campbell, *Defective membrane repair in dysferlin-deficient muscular dystrophy.* Nature, 2003. **423**(6936): p. 168-72.
85. Alderton, J.M.S., R.A. , *How Calcium Influx through Calcium Leak Channels Is Responsible for the Elevated Levels of Calcium-dependent Proteolysis in Dystrophic Myotubes.* Trends Cardiovasc Med, 2001. **10**: p. 268-272.
86. Allen, D.G. and N.P. Whitehead, *Duchenne muscular dystrophy--what causes the increased membrane permeability in skeletal muscle?* Int J Biochem Cell Biol, 2011. **43**(3): p. 290-4.
87. Franco-Obregón, A.L., J.B., *Changes in mechanosensitive channel gating following mechanical stimulation in skeletal muscle myotubes from the mdx mouse.* Journal of Physiology, 2002. **539**(2): p. 391–407.
88. Balijepalli, R.C. and T.J. Kamp, *Caveolae, ion channels and cardiac arrhythmias.* Prog Biophys Mol Biol, 2008. **98**(2-3): p. 149-60.
89. Friedrich, O., et al., *Mini-dystrophin restores L-type calcium currents in skeletal muscle of transgenic mdx mice.* J Physiol, 2004. **555**(Pt 1): p. 251-65.
90. Hirn, C., et al., *Nav1.4 deregulation in dystrophic skeletal muscle leads to Na+ overload and enhanced cell death.* J Gen Physiol, 2008. **132**(2): p. 199-208.
91. Millay, D.P., et al., *Calcium Influx is Sufficient to Induce Muscular Dystrophy Through a TRPC-Dependent Mechanism.* Proceedings of the National Academy of Sciences, 2009. **106**(45): p. 19023-19028.
92. Gailly, P., *TRP channels in normal and dystrophic skeletal muscle.* Curr Opin Pharmacol, 2012. **12**(3): p. 326-34.
93. Hopf, F.W., et al., *A critical evaluation of resting intracellular free calcium regulation in dystrophic mdx muscle.* Am J Physiol, 1996. **271**(4 Pt 1): p. C1325-39.

94. Turner, P.R., et al., *Increased calcium influx in dystrophic muscle.* J Cell Biol, 1991. **115**(6): p. 1701-12.
95. Goonasekera, S.A., et al., *Mitigation of muscular dystrophy in mice by SERCA overexpression in skeletal muscle.* Journal of Clinical Investigation, 2011. **121**(3): p. 1044-1052.
96. Altamirano, F., et al., *Increased resting intracellular calcium modulates NF-kappaB-dependent inducible nitric-oxide synthase gene expression in dystrophic mdx skeletal myotubes.* J Biol Chem, 2012. **287**(25): p. 20876-87.
97. Spencer, M.J., Croall, D. E., & Tidball, J. G. , *Calpains are Activated in Necrotic Fibers from mdx Dystrophic Mice.* . Journal of Biological Chemistry, 1995. **270**(18): p. 10909-10914.
98. Millay, D.P., et al., *Genetic and pharmacologic inhibition of mitochondrial-dependent necrosis attenuates muscular dystrophy.* Nat Med, 2008. **14**(4): p. 442-7.
99. Tantral, L., et al., *Intracellular calcium release is required for caspase-3 and -9 activation.* Cell Biochem Funct, 2004. **22**(1): p. 35-40.
100. Brookes, P.S., et al.. *Calcium, ATP, and ROS: a Mitochondrial Love-Hate Triangle.* American Journal of Physiology-Cell Physiology, 2004. **287**(4): p. C817-C833.
101. Turner, P.R., et al., *Increased protein degradation results from elevated free calcium levels found in muscle from mdx mice.* Nature, 1988. **335**(6192): p. 735-8.
102. Rando, T.A., et al., *Muscle cells from mdx mice have an increased susceptibility to oxidative stress.* Neuromuscul Disord, 1998. **8**(1): p. 14-21.
103. Kumar, A. and A.M. Boriek, *Mechanical stress activates the nuclear factor-kappaB pathway in skeletal muscle fibers: a possible role in Duchenne muscular dystrophy.* FASEB J, 2003. **17**(3): p. 386-96.
104. Mazala, D.A., et al., *SERCA1 overexpression minimizes skeletal muscle damage in dystrophic mouse models.* Am J Physiol Cell Physiol, 2015. **308**(9): p. C699-709.
105. Divet, A. and C. Huchet-Cadiou, *Sarcoplasmic reticulum function in slow- and fast-twitch skeletal muscles from mdx mice.* Pflugers Arch, 2002. **444**(5): p. 634-43.
106. Kargacin, M.E., & Kargacin, G. J. , *The Sarcoplasmic Reticulum Calcium Pump is Functionally Altered in Dystrophic Muscle.* . Biochimica et Biophysica Acta (BBA)-General Subjects, 1996. **1290**(1): p. 4-8.
107. Tupling, A.R., et al., *HSP70 binds to the fast-twitch skeletal muscle sarco(endo)plasmic reticulum Ca2+ -ATPase (SERCA1a) and prevents thermal inactivation.* J Biol Chem, 2004. **279**(50): p. 52382-9.
108. Adachi, T., et al., *S-Glutathiolation by peroxynitrite activates SERCA during arterial relaxation by nitric oxide.* Nat Med, 2004. **10**(11): p. 1200-7.
109. Knyushko, T.V., et al., *3-Nitrotyrosine modification of SERCA2a in the aging heart: a distinct signature of the cellular redox environment.* Biochemistry, 2005. **44**(39): p. 13071-81.
110. Gehrig, S.M., et al., *Hsp72 preserves muscle function and slows progression of severe muscular dystrophy.* Nature, 2012. **484**(7394): p. 394-8.
111. Divet, A., A.M. Lompre, and C. Huchet-Cadiou, *Effect of cyclopiazonic acid, an inhibitor of the sarcoplasmic reticulum Ca-ATPase, on skeletal muscles from normal and mdx mice.* Acta Physiol Scand, 2005. **184**(3): p. 173-86.

112. Schneider, J.S., et al., *Increased sarcolipin expression and decreased sarco(endo)plasmic reticulum Ca2+ uptake in skeletal muscles of mouse models of Duchenne muscular dystrophy.* J Muscle Res Cell Motil, 2013. **34**(5-6): p. 349-56.
113. Voit, A., et al., *Reducing sarcolipin expression mitigates Duchenne muscular dystrophy and associated cardiomyopathy in mice.* Nat Commun, 2017. **8**(1): p. 1068.
114. Bloemberg, D. and J. Quadrilatero, *Rapid determination of myosin heavy chain expression in rat, mouse, and human skeletal muscle using multicolor immunofluorescence analysis.* PLoS One, 2012. **7**(4): p. e35273.
115. Duhamel, T.A., et al., *Muscle metabolic, SR Ca(2+) -cycling responses to prolonged cycling, with and without glucose supplementation.* J Appl Physiol (1985), 2007. **103**(6): p. 1986-98.
116. Muller, J., et al., *Comparative evolution of muscular dystrophy in diaphragm, gastrocnemius and masseter muscles from old male mdx mice.* J Muscle Res Cell Motil, 2001. **22**(2): p. 133-9.
117. Dupont-Versteegden, E.E. and R.J. McCarter, *Differential expression of muscular dystrophy in diaphragm versus hindlimb muscles of mdx mice.* Muscle Nerve, 1992. **15**(10): p. 1105-10.
118. Fajardo, V.A.M., *The Role of Phospholamban and Sarcolipin in Skeletal Muscle Disease.* University of Waterloo, 2017.
119. Chakkalakal, J.V., et al., *Stimulation of calcineurin signaling attenuates the dystrophic pathology in mdx mice.* Hum Mol Genet, 2004. **13**(4): p. 379-88.
120. Michel, R.N., S.E. Dunn, and E.R. Chin, *Calcineurin and skeletal muscle growth.* Proc Nutr Soc, 2004. **63**(2): p. 341-9.
121. McArdle, A., et al., *Contractile activity-induced oxidative stress: cellular origin and adaptive responses.* Am J Physiol Cell Physiol, 2001. **280**(3): p. C621-7.
122. Powers, S.K. and M.J. Jackson, *Exercise-induced oxidative stress: cellular mechanisms and impact on muscle force production.* Physiol Rev, 2008. **88**(4): p. 1243-76.
123. Kho, C., et al., *SUMO1-dependent modulation of SERCA2a in heart failure.* Nature, 2011. **477**(7366): p. 601-5.
124. Sampson, D.A., M. Wang, and M.J. Matunis, *The small ubiquitin-like modifier-1 (SUMO-1) consensus sequence mediates Ubc9 binding and is essential for SUMO-1 modification.* J Biol Chem, 2001. **276**(24): p. 21664-9.
125. Jones, D.H., et al., *Na,K-ATPase from mice lacking the gamma subunit (FXYD2) exhibits altered Na+ affinity and decreased thermal stability.* J Biol Chem, 2005. **280**(19): p. 19003-11.
126. Sweadner, K.J. and C. Donnet, *Structural similarities of Na,K-ATPase and SERCA, the Ca(2+)-ATPase of the sarcoplasmic reticulum.* Biochem J, 2001. **356**(Pt 3): p. 685-704.
127. Heytler, P.G., *uncoupling of oxidative phosphorylation by carbonyl cyanide phenylhydrazones. I. Some characteristics of m-Cl-CCP action on mitochondria and chloroplasts.* Biochemistry, 1963. **2**: p. 357-61.
128. Yap, S.V., et al., *HAX-1: a multifaceted antiapoptotic protein localizing in the mitochondria and the sarcoplasmic reticulum of striated muscle cells.* J Mol Cell Cardiol, 2010. **48**(6): p. 1266-79.
129. De Los Santos, C., et al., *FRAP, FLIM, and FRET: Detection and analysis of cellular dynamics on a molecular scale using fluorescence microscopy.* Mol Reprod Dev, 2015. **82**(7-8): p. 587-604.

130. Kusumi, A., et al., *Tracking single molecules at work in living cells.* Nat Chem Biol, 2014. **10**(7): p. 524-32.

Appendix A

mdx/Pln$^{-/-}$ mice

To generate the *mdx/Pln*$^{+/+}$ and *mdx/Pln*$^{-/-}$ colonies, homozygous female *mdx* animals were crossed with male homozygous *Pln*$^{-/-}$ mice

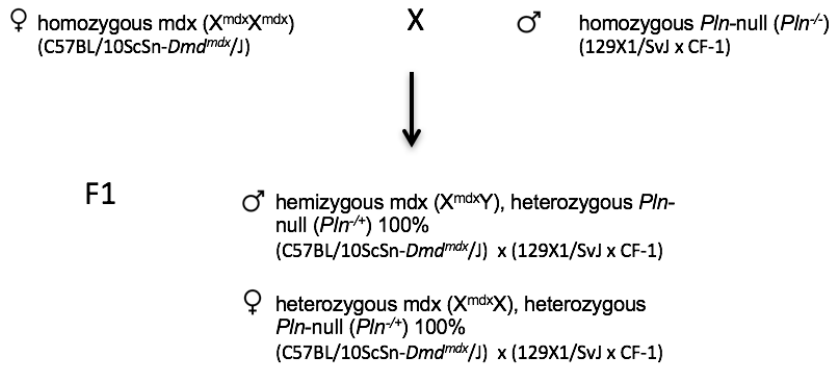

This cross yielded F1 offspring that were either female hemizgous *mdx* or male heterozygous *mdx*. All F1 offspring were heterozygous for *Pln*. Subsequently, F1offspring male and females were crossed together (from a separate breeding pair so that it is not inbred).

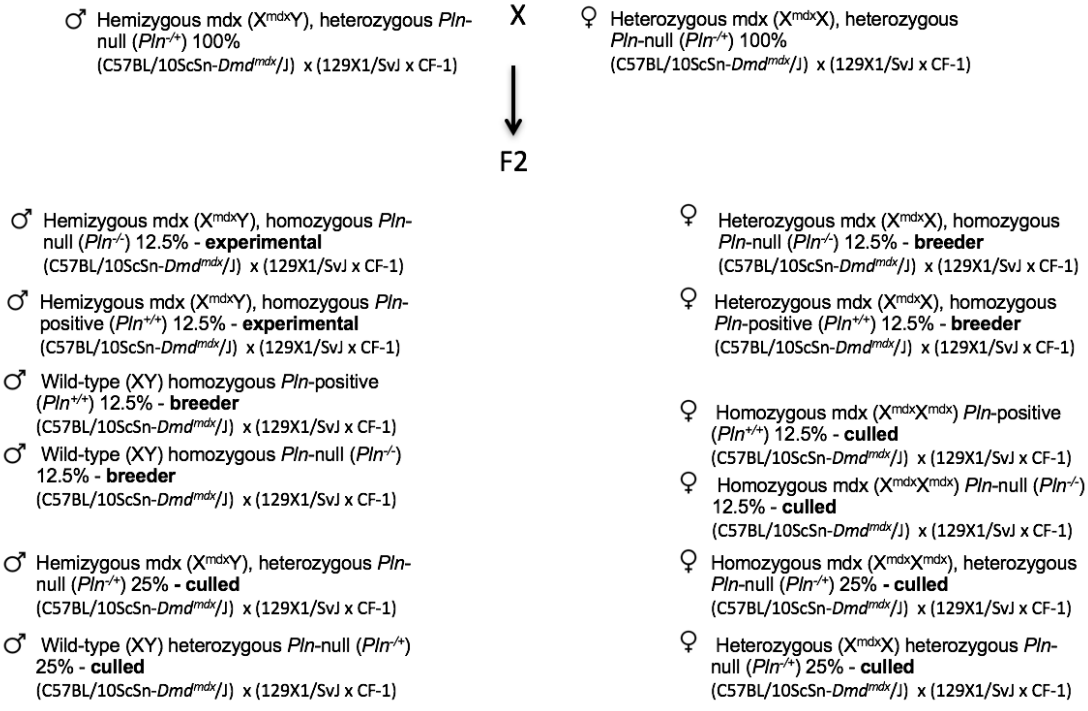

The resulting F2 offspring generated a variety of genotypes, including the experimental groups (*mdx/Pln*$^{+/+}$ and *mdx/Pln*$^{-/-}$). Two subset colonies that independently produced *mdx/Pln*$^{+/+}$ mice and *mdx/Pln*$^{-/-}$ mice were created in order to increases the probability of producing these experimental animals.

mdx/Pln$^{-/-}$: For this subset colony dystrophin positive male mice from F2 were bred with heterozygous *mdx* females from F2, and both sires and dams were homozygous for *Pln*$^{-/-}$.

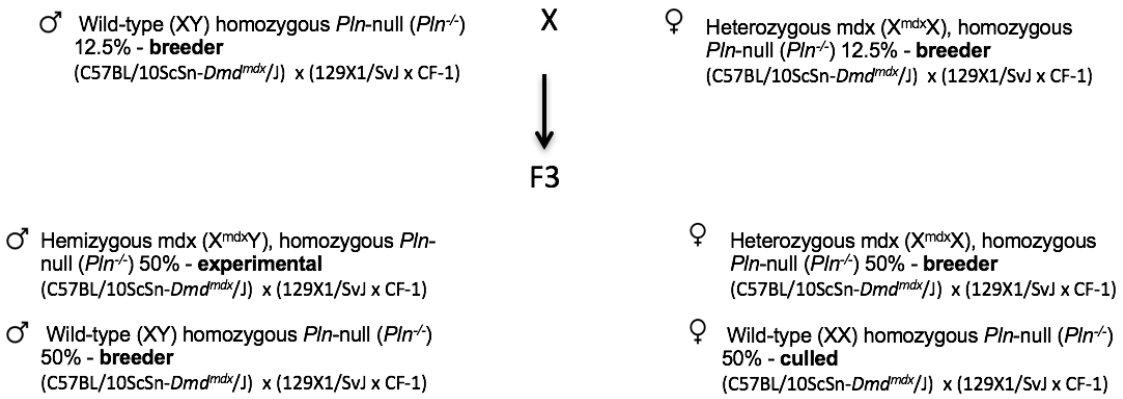

mdx/Pln$^{+/+}$: For this subset colony dystrophin positive male mice from F2 were bred with heterozygous *mdx* females from F2, and both sires and dams were homozygous for *Pln*$^{+/+}$.